ORGANIC PROCESS RESEARCH & DEVELOPMENT
OPR&D

Subscriber access provided by UNIV OF DURHAM

Full Paper

Development of a Large-Scale Route to Glecaprevir: Synthesis of the Macrocycle via Intramolecular Etherification

Jeffrey M. Kallemeyn, Kenneth Michael Engstrom, Matthew Pelc, Kirill Lukin, Westin Morrill, Haojuan Wei, Timothy Towne, Jeremy Henle, Nandkishor Nere, Dennie S Welch, Shashank Shekhar, Matthew Ravn, Gang Zhao, Michael G. Fickes, Chen Ding, John (Cody) Vinci, James Marren, and Russell D Cink

Org. Process Res. Dev., **Just Accepted Manuscript** • DOI: 10.1021/acs.oprd.0c00244 • Publication Date (Web): 13 Jul 2020

Downloaded from pubs.acs.org on July 13, 2020

Just Accepted

"Just Accepted" manuscripts have been peer-reviewed and accepted for publication. They are posted online prior to technical editing, formatting for publication and author proofing. The American Chemical Society provides "Just Accepted" as a service to the research community to expedite the dissemination of scientific material as soon as possible after acceptance. "Just Accepted" manuscripts appear in full in PDF format accompanied by an HTML abstract. "Just Accepted" manuscripts have been fully peer reviewed, but should not be considered the official version of record. They are citable by the Digital Object Identifier (DOI®). "Just Accepted" is an optional service offered to authors. Therefore, the "Just Accepted" Web site may not include all articles that will be published in the journal. After a manuscript is technically edited and formatted, it will be removed from the "Just Accepted" Web site and published as an ASAP article. Note that technical editing may introduce minor changes to the manuscript text and/or graphics which could affect content, and all legal disclaimers and ethical guidelines that apply to the journal pertain. ACS cannot be held responsible for errors or consequences arising from the use of information contained in these "Just Accepted" manuscripts.

is published by the American Chemical Society. 1155 Sixteenth Street N.W., Washington, DC 20036

Published by American Chemical Society. Copyright © American Chemical Society. However, no copyright claim is made to original U.S. Government works, or works produced by employees of any Commonwealth realm Crown government in the course of their duties.

Development of a Large-Scale Route to Glecaprevir: Synthesis of the Macrocycle via Intramolecular Etherification

*Jeffrey M. Kallemeyn, Kenneth M. Engstrom, Matthew J. Pelc, Kirill A. Lukin, Westin H. Morrill, Haojuan Wei, Timothy B. Towne, Jeremy Henle, Nandkishor K. Nere, Dennie S. Welch, Shashank Shekhar, Matthew M. Ravn, Gang Zhao, Michael G. Fickes, Chen Ding, John C. Vinci, James Marren, and Russell D. Cink**

Process Research & Development, and Analytical Research & Development, AbbVie Inc., 1401 Sheridan Road, North Chicago, IL, 60064

For Table of Contents Only (first image is TIFF at 300 dpi, second is chemdraw)

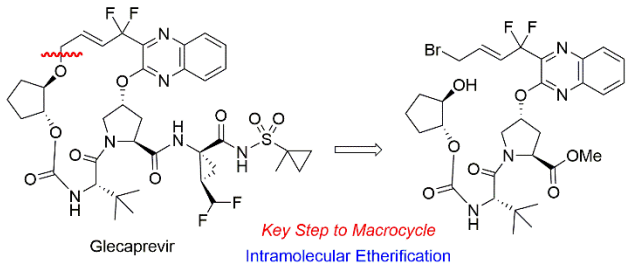

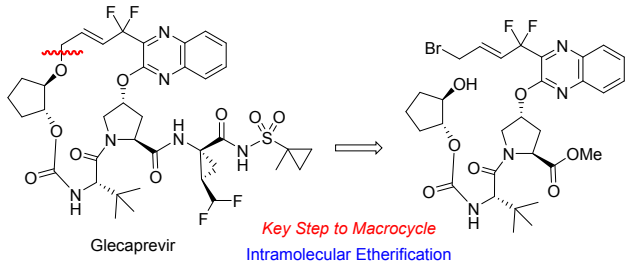

KEYWORDS

glecaprevir, ABT-493, HCV, intramolecular etherification, macrocycle

Abstract: Glecaprevir was identified as a potent HCV protease inhibitor and a large-scale synthesis was required to support the late stage clinical trials and subsequent commercial launch. The large-scale synthetic route to glecaprevir required the development of completely new synthetic approaches to the two key structural features: the 18-membered macrocycle **3**, and the difluoromethyl substituted cyclopropyl amino acid **4**. In this first manuscript, we describe the route development for the macrocycle **3**; the second manuscript will describe the development of a new synthetic route to the difluoromethyl substituted cyclopropyl amino acid **4** and final assembly of glecaprevir. The large-scale synthetic route to the macrocycle employed a unique intramolecular etherification reaction as the key step in the macrocycle synthesis, avoiding the scalability limitations of the RCM reaction of the enabling route. The large-scale synthetic route to the macrocycle was successfully used to produce the amount of glecaprevir required to support the late stage clinical development.

Introduction

Glecaprevir was identified as a potent HCV NS3/4A protease inhibitor, active against all major HCV genotypes.[1] Glecaprevir was developed in combination with pibrentasvir, an NS5A inhibitor which also shows pan-genotypic activity. An enabling synthesis to glecaprevir was employed to support the pre-clinical development and subsequent Phase I clinical trials.[2] The enabling synthesis was suitable to produce the material required for early development, but suffered from two limitations that would hamper the large-scale production required for late stage clinical development.

The initial disconnection in the retrosynthetic analysis for both the enabling route and the large-scale route for glecaprevir (**1**), shown in Scheme 1, dissects glecaprevir into amino sulfonamide **2** and macrocycle **3**. The first limitation of the enabling synthesis was the efficiency

of the ring closing metathesis (RCM) process used to form the macrocycle. The second limitation of the enabling route was the efficiency of the synthesis of the difluoromethyl substituted cyclopropyl amino acid **4**. Based on the scale limitations of the enabling route, it was clear that new syntheses for macrocycle **3** and amino acid **4** would be required for large scale production.[3] The focus of this manuscript is the development of a new route to macrocycle **3**; the new route to amino acid **4** and the final assembly of glecaprevir are the subject of the following manuscript.[4]

Scheme 1: Retrosynthetic Analysis to Glecaprevir

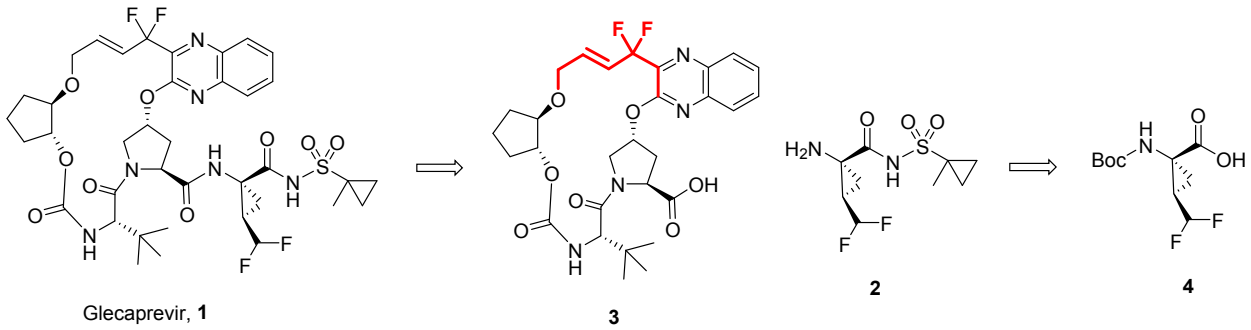

The synthetically challenging structural features to be addressed in the development of a new synthesis for macrocycle **3** are highlighted in red in Scheme 1. A new synthesis of macrocycle **3** posed two related synthetic challenges: a new approach to close the macrocycle, and the construction of the red highlighted six-carbon section of the macrocycle. This six-carbon section contains considerable structural complexity, including an ether, a *trans* alkene, a *gem*-difluoromethylene, and a quinoxaline. The primary synthetic challenge was deemed to be installation of the *gem*-difluoromethylene. Significant advances have recently occurred in the synthesis of substrates containing a *gem*-difluoromethylene.[5] With these challenges in mind, the development of the large-scale synthetic route to macrocycle **3** began.

Results and Discussion

Potential Alternate Routes to the Macrocycle

While multiple approaches to form the macrocycle were considered, the two main disconnection points evaluated, options A and B, are shown in Scheme 2. The appeal of option A was that multiple approaches were possible to form the macrocycle through the bromodifluoroquinoxalines **5-8**. The alkene **5** could undergo an intramolecular Heck reaction to form the macrocycle.[6] The alkyne **6** could undergo a Sonogashira type reaction followed by selective reduction to form the *trans* alkene.[7] Both the alkene **5** and the alkyne **6** could undergo a photoredox catalyzed radical cyclization to form the macrocycle.[8] The alkyne **6** could also be converted to the boronic acid **7** or the boronate ester **8** followed by an intramolecular Suzuki reaction to form the macrocycle.[9] One could also envision switching the order of the bond forming steps, first forming the carbon-carbon bond in an intermolecular coupling and then closing the macrocycle through the lactam. Option B in Scheme 2 involved an intramolecular etherification of the allylic bromide **12**.[10] While etherification with an allylic bromide would normally be considered a straightforward reaction, the probability of success in the formation an 18-membered macrocycle was uncertain.

Scheme 2: Potential Options to Form the Macrocycle

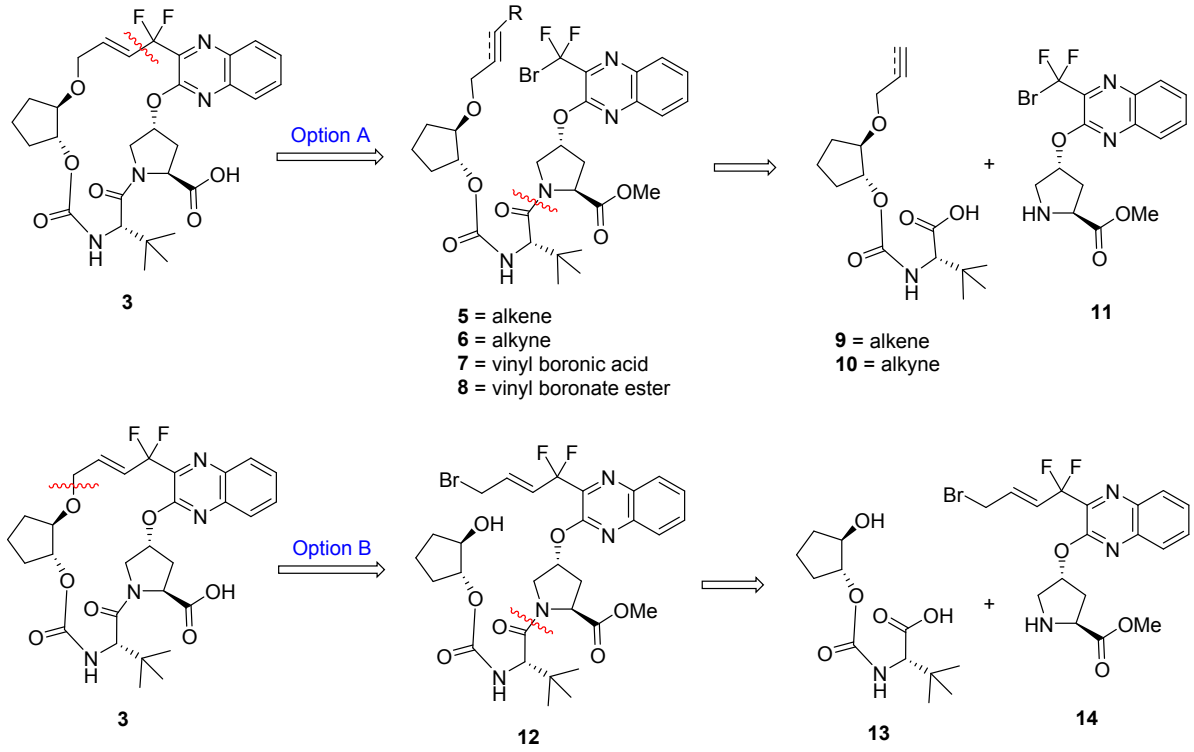

The second key consideration for the synthesis of the macrocycle was the source of the *gem*-difluoromethylene within the six-carbon section highlighted in Scheme 1. Routes that involved fluorination of an advanced intermediate were deemed impractical due to the cost, handling, and limited availability of many fluorination reagents on scale. Instead, the strategy was to develop routes starting from fluorinated building blocks that were commercially available on large-scale. The readily available fluorinated starting material ethyl trifluoropyruvate **17** contained the most complete section of the carbon backbone, as shown Scheme 3 for the retrosynthetic analysis from macrocycle **3**. Elaboration of **17** would involve formation of the requisite carbon-carbon bond with defluorination.

Scheme 3: Retrosynthesis to Fluorinated Starting Material

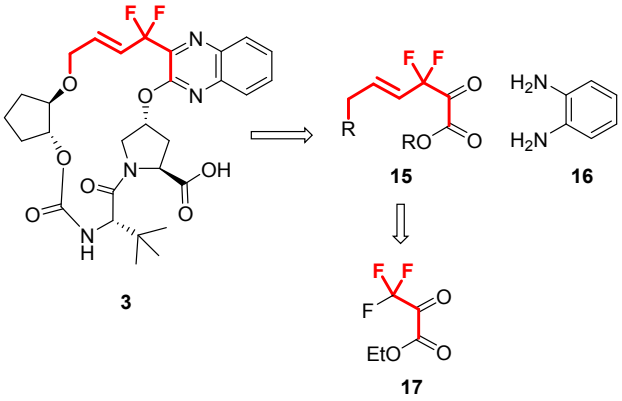

Evaluation of Option A to the Macrocycle

Most of the reactions under consideration for option A in Scheme 2 employed palladium catalysis in the presence of ligand and base. There were significant concerns regarding the stability of the allylic difluoride functionality under these conditions. A stability test of the macrocycle ester **18** to palladium catalysis conditions, shown in Table 1, confirmed these concerns with significant decomposition due to loss of HF in the presence of palladium and ligand (entries 4 and 5). The key challenge for the palladium catalyzed reactions would be identifying conditions in which the desired carbon-carbon forming reaction proceeded significantly faster than the side reaction leading to product decomposition.

Table 1. Stability of Macrocycle Ester **18** to Pd Catalysis Conditions

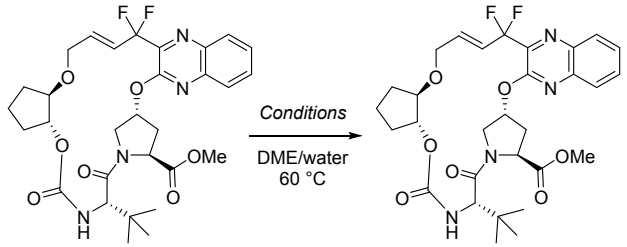

18 18

Entry	$Pd_2(dba)_3$ (equiv)	RuPhos (equiv)	K_3PO_4 (equiv)	Time (h)	Ester **18** HPLC Area %
1	0.05	-	-	16	100
2	-	0.14	-	1	100
3	-	-	2.0	1	92 [a]
4	0.015	0.07	-	1	33
5	0.015	0.07	2.0	1	55

(a) Low levels of ester hydrolysis and epimerization observed.

In order to evaluate the macrocycle synthesis through the option A pathways, the synthesis of bromodifluoroquinoxaline **11** was developed, as outlined in Scheme 4. Condensation of ethyl trifluoropyruvate **17** with diaminobenzene **16** produced quinoxaline **19** in near quantitative yield. The hydrogenation of **19** followed by base treatment proved to be an efficient method to convert the trifluoromethyl quinoxaline **19** to the difluoromethyl quinoxaline **21**. Attempts at alkylation by deprotonation of the difluoromethyl of quinoxaline **22** and related substrates proved to be problematic. The electron withdrawing difluoromethyl group caused the α carbon within the quinoxaline to be exceptionally electrophilic, resulting in dimerization of **22** during deprotonation. Interestingly, the only electrophile identified that could be cleanly trapped by the anion of quinoxaline **22** was brominating agent **23**; facilitating the unique bromination for the conversion of difluoromethyl quinoxaline **22** to the bromodifluoromethyl quinoxaline **24**. Slow addition of LiHMDS (3 equiv) to a solution of quinoxaline **22** and bromine (2 equiv) induced in situ formation of brominating agent **23**, followed by deprotonation of the difluoromethyl group

and trapping of the resulting anion by **23**. The synthesis of **11** was completed by S_NAr reaction of quinoxaline **24** with hydroxyproline **25** followed by deprotection. The overall yield of 66% for the seven-step sequence to produce **11** was very encouraging for this approach.

Scheme 4: Synthesis of Bromodifluoroquinoxaline **11**

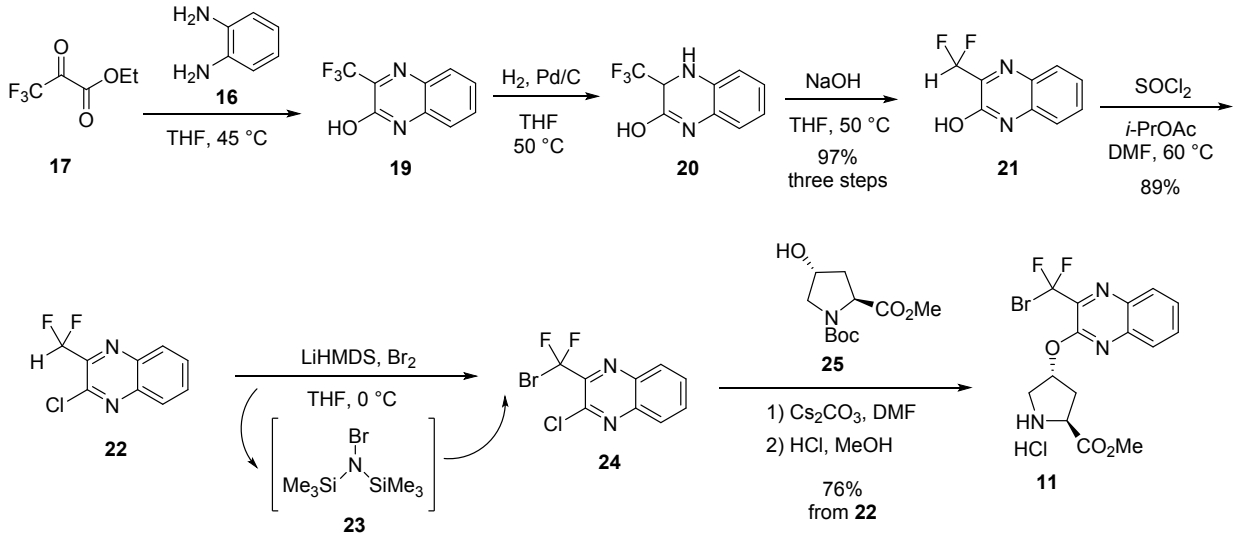

Completion of the synthesis of the substrates for evaluation of the option A cyclization strategies followed the general strategy outlined in Scheme 2.[11] A significant amount of screening was conducted for the cyclization methods of option A, and selected results are summarized in Scheme 5. Screening of the intramolecular Heck reaction of alkene **5** (Scheme 2) revealed the main product formed was consistent with cyclization followed by loss of HF. A similar result was observed in the intramolecular Sonogashira type reaction of alkyne **6**; however, conversion was low. The intramolecular Suzuki reaction of boronate ester **8**, shown in Scheme 5, was screened extensively. The best results were obtained with sterically hindered phosphine ligands such as P(*t*-Bu)$_3$ and RuPhos, but the yield reached a maximum of 11% due to significant product decomposition from loss of HF.[12] The boronic acid **7** did not offer any improvement. The intramolecular photoredox catalyzed cyclization reaction of alkene **5** was not

successful, but a low yield of **18** was observed using the boronic acid **7**. The best result for the photoredox cyclization was obtained with alkyne **6**, shown in Scheme 5, which produced a 30% yield of macrocycle **18** in a 2:1 ratio of *trans/cis* alkene isomers. A model vinyl boronate ester **26** was used to evaluate the intermolecular Suzuki reaction with bromodifluoroquinoxaline **27**.[13] Under nickel catalysis, negligible cross coupling occurred, along with up to 10% of homocoupling of **27**.[14] Under palladium catalysis, the reaction showed rapid conversion to the coupled product **28**, but also significant decomposition through loss of HF. The addition of CsF (2 equiv) was found to minimize impurities from the loss of HF to approximately 5%, and the addition of water (1 equiv) resulted in faster conversion and improved product yield. The best result obtained for the intermolecular Suzuki coupling was a 62% assay yield for **28**, demonstrating the feasibility of this approach to form the desired carbon-carbon bond. The challenge for this approach would be the narrow operating window between achieving reaction completion and over reaction with loss of HF resulting in erosion of the product yield. This intermolecular Suzuki approach, in combination with subsequent macrocycle closure through the lactam, was deemed a feasible approach to form the macrocycle; but the product stability under the cross-coupling reaction conditions was recognized as a liability for large-scale production.

Scheme 5: Select Results for Option A Trials

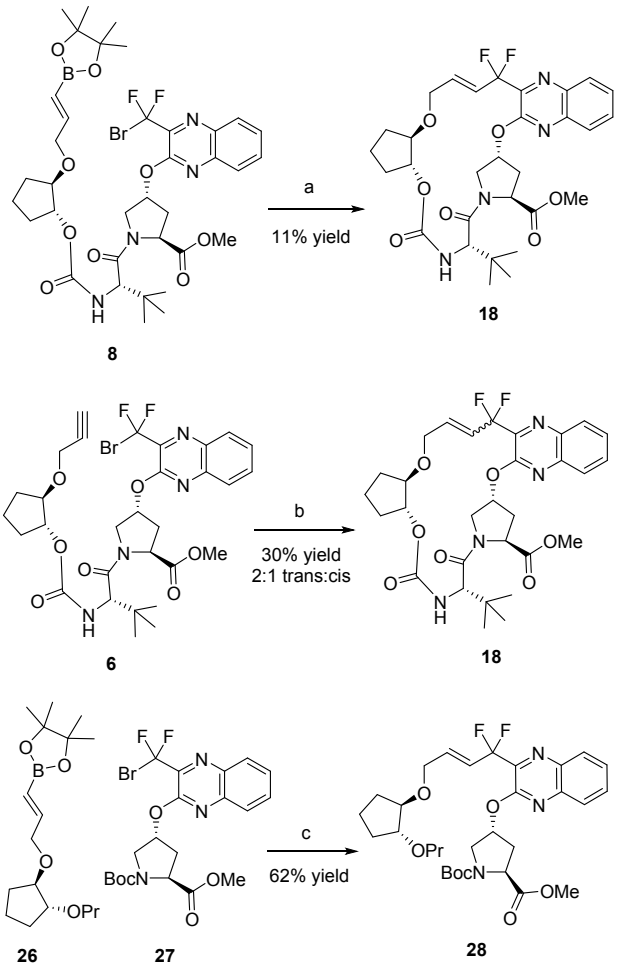

Reagents and Conditions: (a) $Pd_2(dba)_3$ (1.5 mol%), RuPhos (3.6 mol%), K_3PO_4 (2 eq), DME/water (20:1), 50 °C. (b) $Ru(bpy)_3$ (1 mol%), $CH_3(CH_2)_{11}SH$ (1.5 eq), DIPEA (2 eq), 4:1 toluene:CH_3CN, 32 °C, blue LEDs. (c) $Pd_2(dba)_3$ (1.5 mol%), RuPhos (3.6 mol%), K_3PO_4 (2 eq), CsF (2 eq), H_2O (1 eq) DME, 50 °C.

Evaluation of Option B to the Macrocycle

In order to test the option B cyclization shown in Scheme 2, the synthesis of allylic bromide **12** was undertaken starting with intermediates available from the RCM reaction of the enabling route.[15] As shown in entry 1 of Table 2, the initial cyclization experiment utilized 40% aqueous benzyltrimethylammonium hydroxide (Triton® B) as base and revealed the cyclization proceeded cleanly; yielding the desired macrocycle **3** and a lower level of impurity **29**.

Interestingly, S_N2' cyclization was not observed; rather impurities **29** and **30** were formed through cyclization of the carbamate.[16] A solvent screen (entries 2-5) revealed that the use of a biphasic toluene/water system produced a 74% combined assay yield for the macrocycle **3** and the macrocycle ester **18**, with very low levels impurities **29** and **30**. This result demonstrated the feasibility of the intramolecular etherification approach to form the macrocycle. In fact, the assay yield for this early result was already superior to the RCM reaction of the enabling route.[2] Additionally, the product was isolated in > 99.5% purity upon crystallization. With these results in hand, the focus shifted to developing the synthesis of allylic bromide **12**.

Table 2. Initial Cyclization Results of Option B

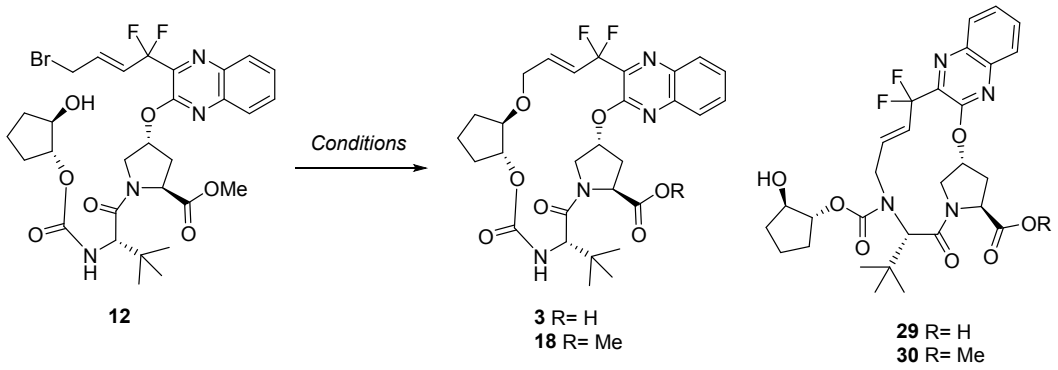

Entry	Solvent	Solvent Volumes	$BnMe_3NOH$ (equiv.)	Time (h)	Assay Yield %[a]	HPLC Area %			
						3	**18**	**29**	**30**
1	THF	10	2.8	13	51	57	-	29	-
2	NMP	10	1.2	2.7	-	-	-	6	76
3	MTBE	10	1.2	20	39	72	-	10	-
4	Toluene	20	2.6	16	57	58	10	8	4
5	Toluene/water (2:1)	30	10	15	74	78	4	5	1

(a) Combined assay of **3** and **18**.

Retrosynthesis of Allylic Bromide 12

The retrosynthesis of allylic bromide **12**, shown in Scheme 6, initially dissects the amide bond of **12** into carbamate **13** and allylic bromide **14**. The carbamate **13** could be synthesized from alkene **9**, an intermediate in the enabling route to glecaprevir.[2] To minimize potential side

reactions from carrying allylic bromide **14** through multiple steps, the alcohol **31** was considered as a potential masking group for subsequent conversion to the bromide. Intermediates **14** or **31** could be derived through an S_NAr reaction of a protected hydroxyproline with quinoxaline **32** followed by an allylic bromination or oxidation with transposition of the alkene. Quinoxaline **32** could be readily prepared from the known keto ester **33**.[17] The majority of steps in the retrosynthesis to **12** were perceived to have a high probability of success, but the allylic bromination or oxidation with alkene transposition was considered to be challenging due to the presence of the *gem*-difluoromethylene.

Scheme 6: Retrosynthesis of Allylic Bromide **12**

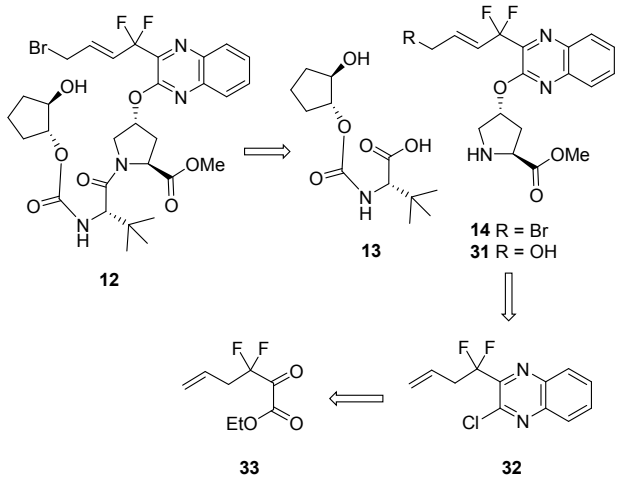

Synthesis of Carbamate 13

The synthesis of carbamate **13**, shown in Scheme 7, was based on the synthesis of alkene **9** which was previously described in the enabling route to glecaprevir.[2] The isolation of **9** as the dicyclohexylamine salt was eliminated from the process, and the subsequent deallylation of **9** proceeded as expected, with carbamate **13** isolated as the diisopropylamine (DIPA) salt. The robust six-step sequence produced carbamate **13** in 26% yield from cyclopentene oxide **34**.

Scheme 7: Synthesis of Carbamate **13**

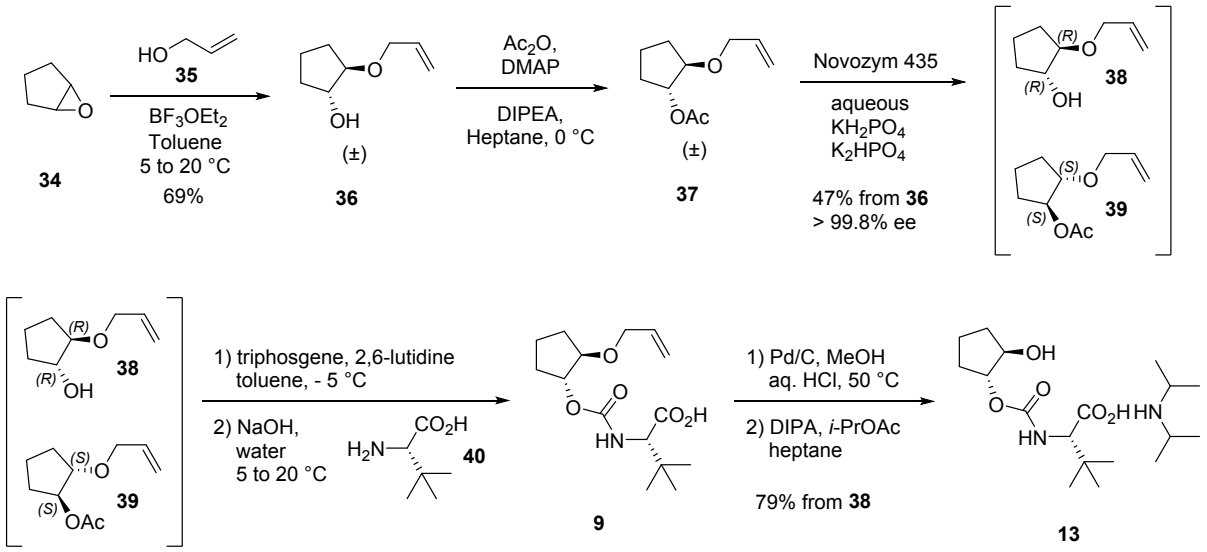

Synthesis of Quinoxaline 32

The synthesis of quinoxaline **32**, shown in Scheme 8, began with the known synthesis of keto ester **33**.[17] While the route to **33** was already established, some unique aspects of the large-scale synthesis are worth discussion. The starting pyruvate **17** contains a low level of the corresponding fluorohydrin impurity which can release HF upon reaction with allyl alcohol. To avoid the potential for HF corrosion, pyridine was charged to the reactor prior to the addition of **17**, and upon completion the reaction was quenched into aqueous base to avoid an acidic pH environment. To ensure a reproducible activation of Zn with TMSCl, the oxygen level was controlled below 50 ppm and the slurry mixed for at least 90 minutes after the TMSCl addition. A portion-wise addition of the activated Zn slurry to chloride **41** was important to control the reaction temperature and minimize impurities formed by over-reduction. The reactor set up, shown in Figure 1, utilized recirculation of the Zn slurry in DMF with the return diptube near the bottom of the reactor and angled to create a vortex. This facilitated nearly complete transfer of the slurry when the volume dropped below the agitator. The slurry was recirculated throughout the deoxygenation and activation, and subsequently portions of the Zn slurry were added to the

second reactor containing chloride **41**. After filtration of the slurry, the solution was heated to induce the Claisen rearrangement and followed by condensation with diaminobenzene **16** to form the quinoxaline **43**. The Zn reduction also generates fluoride and consequently was also a potential source of corrosion. Quenching the condensation reaction with aqueous NH_4Cl induced crystallization of quinoxaline **43**, ensured solubility of the Zn salts, and produced a mixture that was not corrosive to stainless steel. A straightforward chlorination and subsequent crystallization completed the synthesis of quinoxaline **32**.

Scheme 8: Synthesis of Quinoxaline **32**

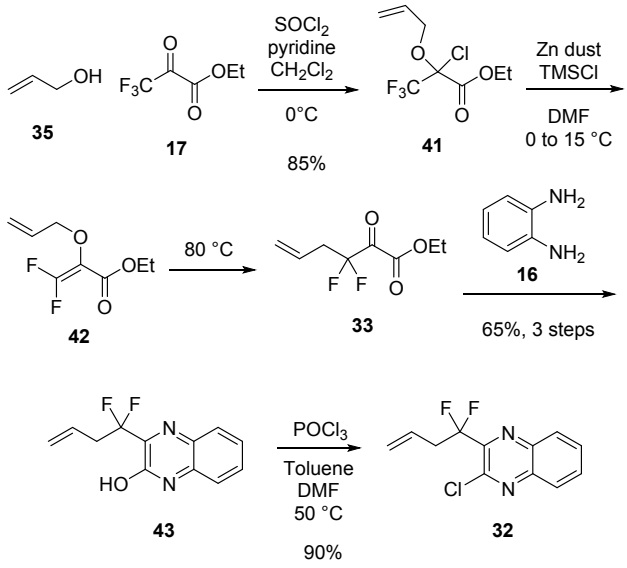

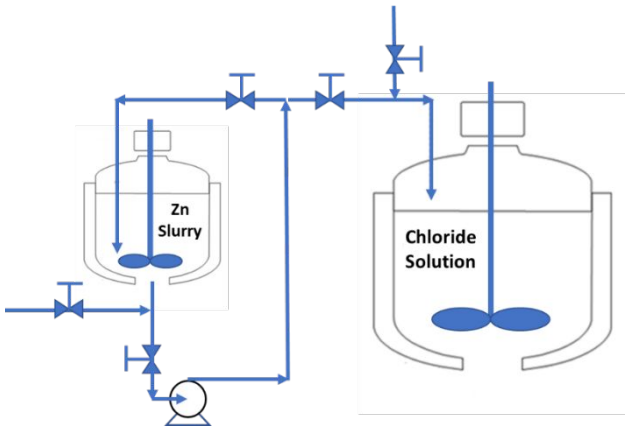

Figure 1. Reactor Configuration for Zn Reduction

Methods for Allylic Functionalization with Transposition

Numerous methods were evaluated to perform the allylic functionalization with transposition on quinoxaline **32** and similar substrates. Mild halogenation conditions resulted in no conversion, whereas forcing conditions to activate the alkene induced intramolecular attack of the quinoxaline nitrogen to form 5-membered cyclic impurities. The allylic oxidation conditions of White were successful, but the product yield and purity were too low for large-scale production.[18] Ultimately, epoxidation and dihydroxylation were the only methods found to cleanly oxidize the alkene of quinoxaline **32** and related substrates. As outlined in Scheme 9, the epoxide **44** or the diol **45** could be converted to the allylic alcohol **31**. As outlined in Scheme 6, allylic bromide **14** or allylic alcohol **31** were possible intermediates in the synthesis of **12**. Based on the required intermediacy of allylic alcohol **31**, the strategy was to conduct the subsequent conversion to the allylic bromide after the coupling of **31** with carbamate **13**. Both the epoxidation and dihydroxylation approaches were evaluated for the synthesis of the macrocycle.

Scheme 9: Options for Allylic Oxidation with Transposition

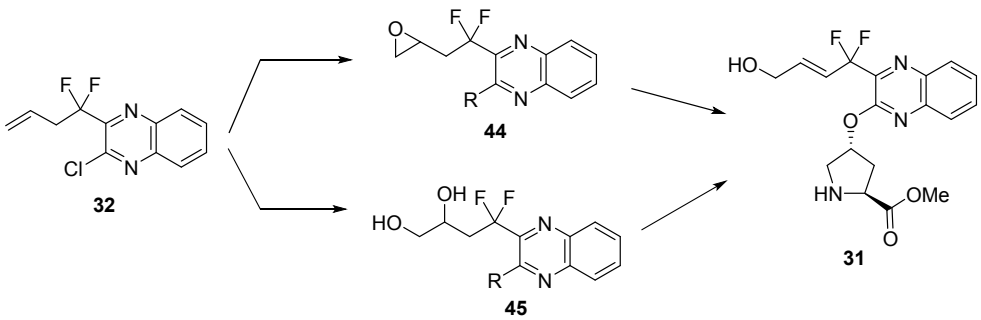

Epoxidation Route to Allylic Alcohol 31

The epoxidation route began with the S_NAr reaction of quinoxaline **32** with hydroxyproline **46** using NaH as the base.[19] Numerous bases were screened for the synthesis of ether **47**; elimination of HF was a significant side reaction resulting in low yield and purity for bases other

than NaH. After considerable development, the epoxidation method of Yang was successfully applied to synthesize epoxide **48**.[20] The epoxide was unstable under acidic conditions, requiring a careful workup and isolation as a solution of the sodium salt. The epoxide ring opening performed acceptably with LiHMDS, however potassium *tert*-amylate (KOtAm) provided a slightly improved yield. Elimination of HF was also a side reaction in the epoxide opening, resulting in oligomer formation that required a DMEDA quench and complex workup to yield a stable product solution. The epoxide opening also produced 7.2% of the *cis* alkene isomer impurity. After considerable screening, crystallization of **49** as the benzhydrylamine (Ph_2CHNH_2) salt was identified and facilitated isolation of allylic alcohol **49** in 63% yield. After a salt break, treatment of allylic alcohol **49** with a solution of thionyl chloride in methanol allowed simultaneously esterification of the carboxylic acid and deprotection of the amine resulting in clean formation of **31** in high yield and purity.

Each of the first three steps in Scheme 10 had liabilities for large-scale production: the use of NaH in the first step; the throughput, Oxone® waste, and product stability in the second step; and the modest yield and impurity formation in the third step. The epoxidation route produced allylic alcohol **31** in 40% overall yield from quinoxaline **32**, but the above-mentioned liabilities were recognized as a challenge for continued large-scale production.

Scheme 10: Epoxidation Route to Allylic Alcohol **31**

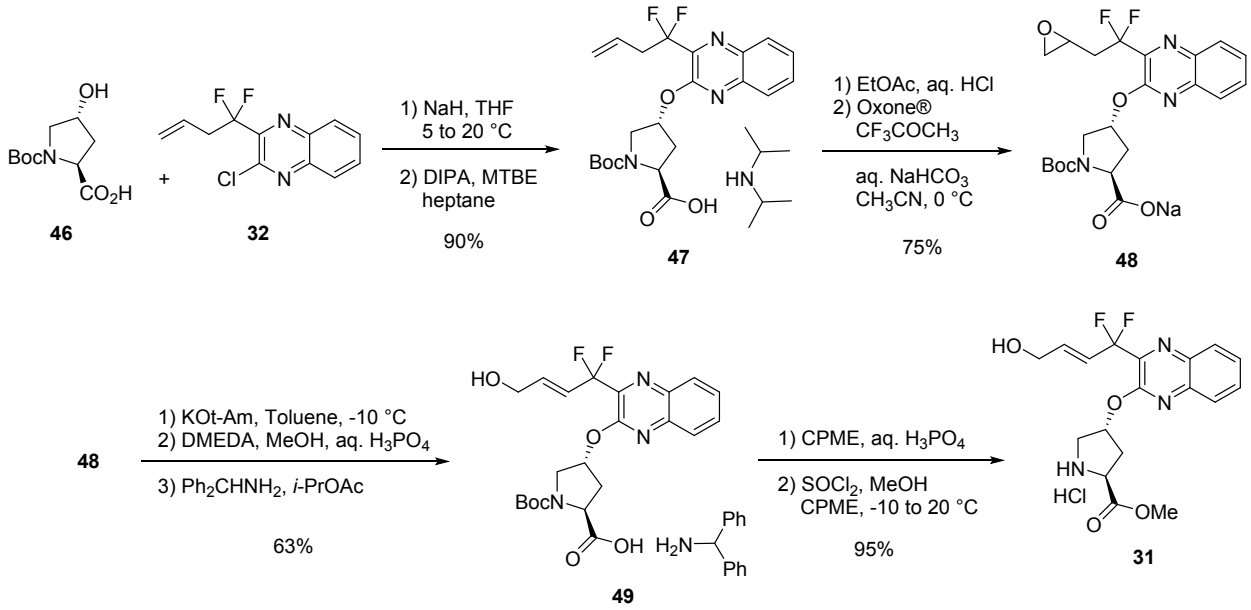

Dihydroxylation Route to Allylic Alcohol 31

The dihydroxylation route to allylic alcohol **31** is shown in Scheme 11. The dihydroxylation of quinoxaline **32** was found to be very robust and required only 0.15 mol% of potassium osmate dihydrate catalyst and aqueous NMO as the oxidant.[21] The subsequent conversion to the cyclic carbonate **50** with CDI was also robust resulting in a 90% overall yield from **32**. The conversion of cyclic carbonate **50** to allylic alcohol **49** was accomplished in a two-step, one-pot process. Treatment of **50** with NaHMDS at –5 °C afforded the open carbonate **51**, which serves as a transient protecting group for the allylic alcohol. We were pleasantly surprised to find that the open carbonate **51** was sufficiently stable to allow the S_NAr reaction to proceed cleanly upon addition of a slurry of the dianion of hydroxyproline **46**. Another positive observation for the carbonate opening was the level of the *cis* alkene isomer was only 0.5%, a significant reduction from the 7.2% observed in the epoxide opening. After an aqueous workup and carbon treatment, allylic alcohol **49** was isolated by crystallization as the benzhydrylamine salt.

Scheme 11: Dihydroxylation Route to Allylic Alcohol **31**

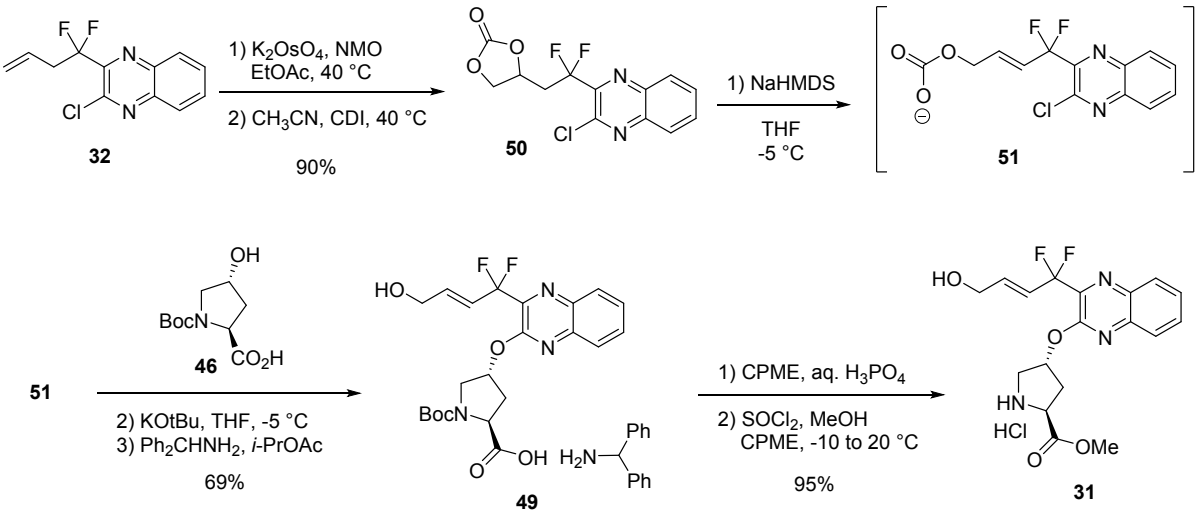

A variety of bases were screened for the carbonate opening and NaHMDS and LiHMDS gave the cleanest profiles. The alkoxide bases (NaOtBu, KOtBu, KOtAm) all gave numerous impurities. LiHMDS gave a clean profile and good assay yield for the carbonate opening, but the resulting lithium carbonate gave a slow conversion in the S_NAr reaction and higher impurity levels. The carbonate opening reaction was found to be essentially instantaneous; the NaHMDS reacting immediately with the cyclic carbonate **50** to produce the open carbonate **51** in typically 92-100% assay yield. While the carbonate opening reaction was not particularly temperature sensitive, it was exothermic with an adiabatic temperature rise of 22 °C. Therefore, the carbonate opening was conducted at -5 °C. Any excess base resulted in a lower assay yield for the reaction; believed to be a result of open carbonate **51** decomposition, possibly through elimination of HF.

A base screen for the S_NAr reaction revealed that NaHMDS, NaOtBu, and KOtBu were the best options, giving complete conversion of the open carbonate and assay yields of 78-90%. The use of KOtBu resulted in a slightly higher assay yield and a faster reaction when compared to NaOtBu. The addition of a small amount of water to the slurry of KOtBu and hydroxyproline **46** was found to have a positive impact on the yield of the S_NAr reaction. The exact role of the water

added to the hydroxyproline **46** slurry remains unclear; however, it may serve to reduce the basicity of the reaction mixture by formation of KOH and/or KOTMS. Reactions devoid of water had lower yields than those with water deliberately charged.

The main process impurity formed in this reaction was the dimer **54**, with the proposed pathway shown in Table 3.[22] Throughout the course of development, the parameters impacting the level of dimer **54** were found to be the addition time of the dianion slurry, the total amount of water in the slurry preparation, and the S_NAr reaction temperature during the slurry charge. These parameters were studied in a multivariate fashion, with the results summarized in Table 3. Based on these results, the process was conducted with an addition time as short as possible while maintaining the S_NAr reaction temperature and the water content within the targeted range. With control of these reaction parameters, the allylic alcohol **49** was routinely isolated in 69% yield as the benzhydrylamine salt. Conversion of **49** to **31** was accomplished as described earlier for the deprotection and methyl ester formation. The overall yield of allylic alcohol **31** from quinoxaline **32** was 59% for the dihydroxylation route, a significant improvement over the 40% for the epoxidation route.

Table 3. Proposed Pathway and Multivariate Study on the Formation of Dimer **54**

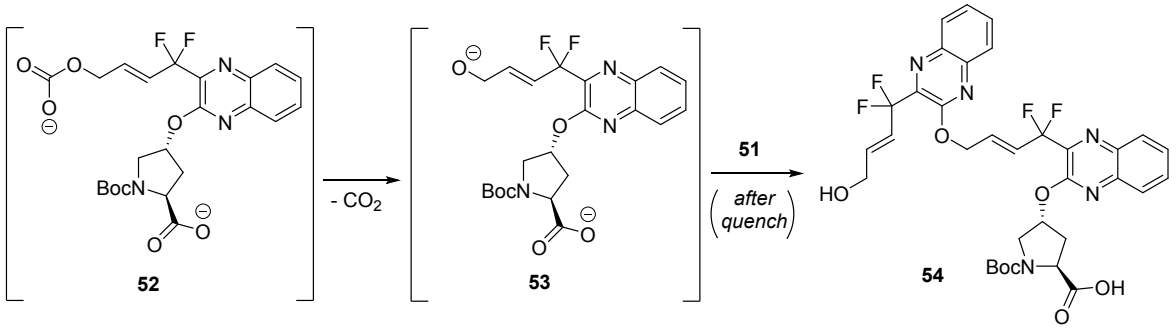

Entry	Water Amount (kg/kg **50**)	Addition Time (h)	S_NAr Temp.[a] (°C)	Dimer **54** [b] (HPLC area %)	Assay Yield
1	0.025	0.05	-10	2.5	71.9%
2	0.031	0.05	-10	2.8	71.3%
3	0.036	0.05	-10	4.9	69.7%
4	0.029	0.07	5	6.3	65.2%
5	0.031	6.5	-15	7.6	62.1%
6	0.036	5.4	0	13.0	N/A [c]
7	0.031	7.3	0	13.9	41.1%

(a) Temperature of the S_NAr reaction during the addition of the slurry of **46**. (b) Level in the reaction completion sample. (c) Not measured.

Determining the Origin of Selectivity in Allylic Alcohol Formation

To determine why the carbonate opening leads to higher *trans* selectivity than the epoxide opening, a computational study was undertaken. To simplify the calculation, the epoxide was modeled using the chloride substrate **56** shown in Scheme 12, consistent with the cyclic carbonate **50**. Additionally, counter-ion effects were ignored (and the counter ions not included in the calculation). The Supporting Information details the methods used for the computational analysis.

Scheme 12: Substrates Investigated in the Computational Study

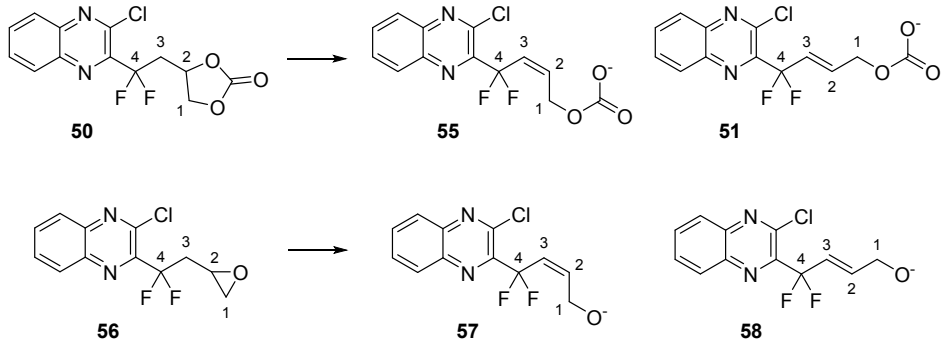

Transition states leading to *cis* and *trans* products were located for both substrates. In the carbonate system, the transition state leading to the *cis* product was found to be 4.4 kcal/mol higher in energy than the transition state leading to the *trans* product. This would correspond to a >4000:1 selectivity for the *trans* isomer, which is larger than observed experimentally (Table 4, entry 2), but within computational error.[23] In the epoxide system, the transition state leading to the *cis* isomer was found to be only 0.4 kcal/mol higher in energy than the *trans* isomer, corresponding to a 2.3:1 selectivity for the *trans*. The difference between the calculated and experimental selectivity observed with the epoxide (Table 4, entry 1) can be rationalized by the increased steric bulk in the region of interest for epoxide **48** compared to the model epoxide **56**.

Table 4. Calculated versus Observed Levels of Olefin Isomers

Entry	Substrate	Calculated *trans:cis*	Observed *trans:cis*
1	Epoxide **56**	2.3:1	12.9:1
2	Cyclic Carbonate **50**	4000:1	200:1

The transition states identified for both substrates show significant E2 character, with shortening of the C2-C3 bonds, hybridization of the carbon atoms in the forming olefin, and the lengthening of the carbonate C1-O bond (Figure 2 and Figure 3). The degree of hybridization in the carbon being deprotonated suggests the transition state is early, and that the elimination itself is asynchronous, with significant negative charge accumulation on the deprotonated carbon.

Additionally, the neighboring C3-C4 bond is also shortened, evidence of negative hyperconjugation between the developing anion and the σ* of the antiperiplanar C-F bond. This stabilizing interaction is observed in both the *cis* and *trans* transition states for each substrate, and the bond lengths suggests a similar amount of partial double bond character along the forming olefin and C3-C4 bond.

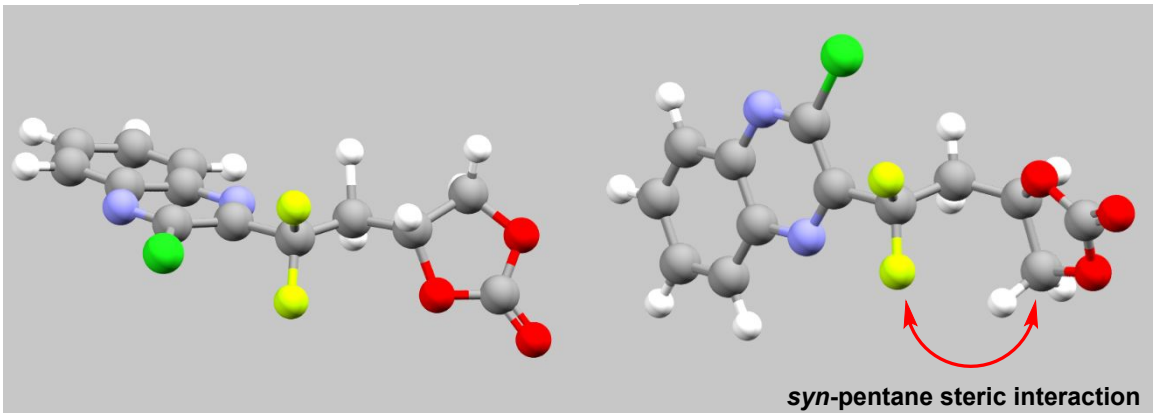

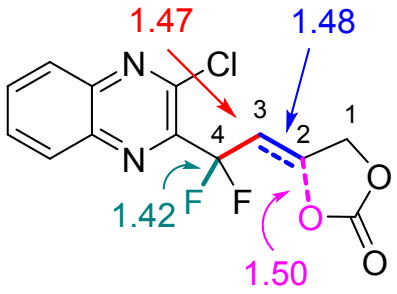

carbonate-TS *trans*

$\Delta\Delta G^{\ddagger}_{rel}$ = 0 kcal/mol

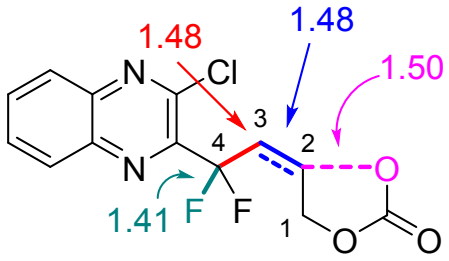

carbonate-TS *cis*

$\Delta\Delta G^{\ddagger}_{rel}$= 4.4 kcal/mol

Figure 2. Carbonate transition states with steric interactions highlighted. Left: transition state leading to the *trans* isomer. Right: transition state leading to the *cis* isomer. Bottom: Bond lengths (reported in angstroms) for both transition states. The base has been omitted for clarity.

The largest contributor to the energy difference between the *cis* and *trans* isomers for the carbonate substrate appears to be a *syn*-pentane-like steric interaction between one of the fluorine atoms and the terminal carbon of the carbonate (Figure 2). The orbital overlap requirements for the elimination and the stabilizing interactions with the C-F bond forces the pro-*cis* carbonate transition state into a conformation that exhibits a *syn*-pentane like interaction between C1 and

one of fluorine atoms on C4, resulting in increased steric interaction. In the pro-*trans* case, the interaction is lessened to the fluorine experiencing steric interaction with a hydrogen atom. The difference in steric interaction alone is enough to account for the 4.4 kcal/mol energy difference.

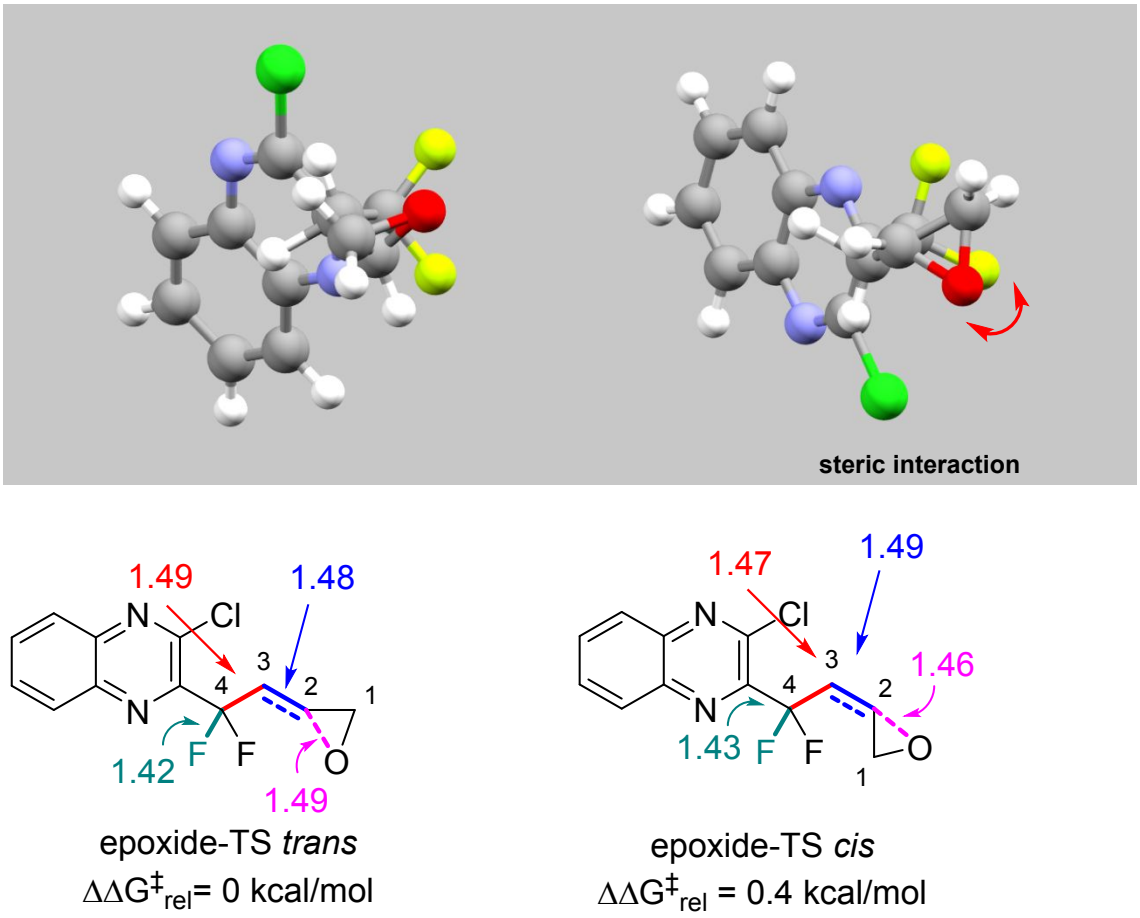

Figure 3. Epoxide transition states. Left: transition state leading to the *trans* isomer. Right: transition state leading to the *cis* isomer. Bottom: Bond lengths (reported in angstroms) for both transition states. The base has been omitted for clarity.

In the epoxide substrate (Figure 3), this type of steric interaction is not observed due to the bond angles of the epoxide. Instead of the carbon experiencing *syn*-pentane like interactions, C1 is staggered between the fluorine atoms, avoiding the steric strain. In the pro-*cis* transition state, there is some interaction between the epoxide oxygen and one of the fluorine atoms (Figure 3, right), which explains the transition state being 0.4 kcal/mol higher in energy.

Strategy for the Synthesis of Macrocycle 3

The key observation of the facile ring closure of the allylic bromide **12** to the macrocycle **3** (Table 2) led to the development of the process to couple allylic alcohol **31** and carbamate **13** to afford the diol **59**, outlined in Scheme 13. The selective conversion of the diol **59** to the allylic bromide **12** would set the stage for the key ring closure. For a highly functionalized molecule, special attention would need to be paid to the selectivity of the reactions, impurity formation and impurity rejection. The impurity profile of macrocycle **3** would need to be well understood as it is the penultimate intermediate for the synthesis of glecaprevir and any impurities in this stage could impact the final quality of the drug substance.

Scheme 13: Macrocycle **3** Synthetic Route

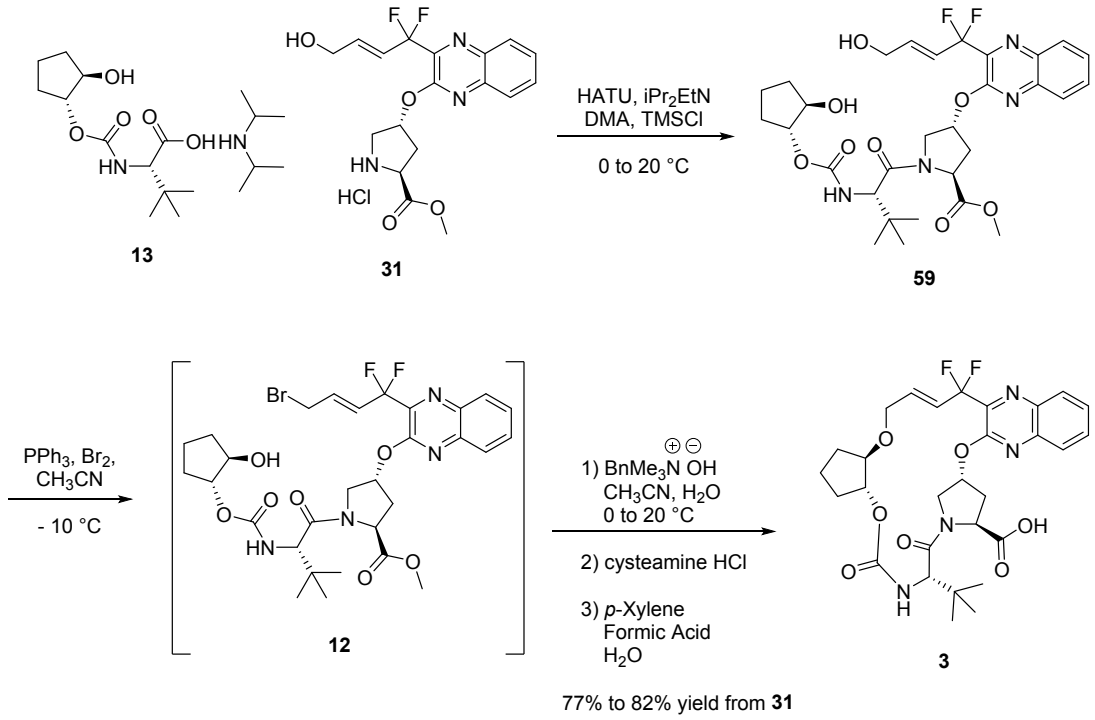

13 31 59 12 3

As the development of these stages progressed, it was apparent that isolation of the diol **59** or the allylic bromide **12** would be challenging due to less than ideal physical properties of the intermediates, and in this regard a telescoped process was targeted. The development of a

telescoped process then added the requirement that the process streams be compatible with the next step. From the enabling route, it was known that the crystallization of the macrocycle **3** provided significant purification, and this isolation was targeted as a key control point for rejection of process impurities.

Development of the Coupling

The best conditions identified for the coupling of allylic alcohol **31** with carbamate **13** utilized DIPEA as the base, HATU as the acid activation agent, and DMA as the solvent. Under these conditions the formation of a side product resulting from the acylation of the allylic alcohol was also observed to the extent of 5%. It was possible to reduce this side reaction via pretreatment of **31** with TMSCl, causing in situ protection of the allylic alcohol. Less than 1% of the side product was formed when the process was conducted under these improved conditions. After an extractive workup with toluene and a solvent switch to acetonitrile, the solution of diol **59** was used directly in the bromination step.

Development of the Bromination

With the diol intermediate **59** in hand, a method was needed to selectively transform the allylic alcohol to the allylic bromide in the presence of other functionality, including a secondary alcohol. While a number of conditions are available for this transformation, the selectivity imparted by the use of phosphonium reagents was quite attractive for further development.[24]

The bromination reaction was initially developed to isolate a crude solution of **12**. Conversion of **59** to **12** could be affected by bromination using PPh_3Br_2 in DCM. The reaction mixture needed to be quenched into vigorously stirred aqueous $NaHCO_3$ to prevent bromination of the secondary cyclopentyl alcohol that was observed during extended reaction times and at higher temperatures. These issues on workup could be solved by telescoping the reaction quench

directly into the cyclization reaction. This telescoped process was facilitated by changing the solvent from DCM to the aqueous miscible MeCN.

The bromination reaction was found to be sensitive to water, resulting in lower conversion and decreased purity. To minimize exposure to moisture, the PPh_3Br_2 reagent was prepared *in situ* by addition of Br_2 to a fine suspension of PPh_3 in MeCN. The cleanest bromination reactions used a slight excess of Br_2 in the formation of the PPh_3Br_2 reagent. The resulting PPh_3Br_2 slurry (1.25 equiv) was added to the solution of diol **59** at -10 °C. The reaction was exothermic, and the transfer was conducted at a rate to maintain an internal temperature below 0 °C. The solution of allylic bromide **12** was used directly in the cyclization reaction.

Development of the Cyclization Reaction

A strong base, such as hydroxide, was necessary for the cyclization of **12** to **3** (Table 5). Under the reaction conditions, saponification occurred at a faster rate than the cyclization, with uncyclized bromo-acid intermediate **60** being the last species to cyclize and as such was used for monitoring for reaction completion. A base screen was conducted (Table 5) and the use of a quaternary ammonium counterion, such as with Triton® B ($BnMe_3NOH$), showed a significantly faster reaction rate when compared to LiOH, NaOH or KOH. Additionally, the use of Triton® B also minimized the amount of hydrolysis of the allylic bromide to the diol impurity **61**. An attempt to minimize the amount of Triton® B did not show any improvement; combination of 1 equiv of Triton® B with 4 equiv of KOH was slower with higher formation of diol **61** than Triton® B alone.

Table 5. Base Screen for the Cyclization of Allylic Bromide **12**

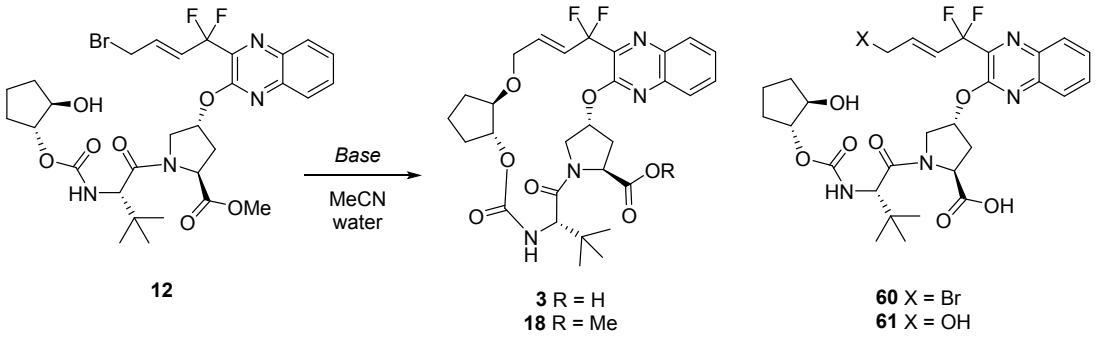

12

3 R = H
18 R = Me

60 X = Br
61 X = OH

Entry	Base	Equiv	Time (h)	HPLC Area %				
				12	**3**	**18**	**60**	**61**
1	Triton® B	5	19	0	86	0	3.5	3.4
2	KOH	5	23	15	12	13	50	3.5
3	NaOH	5	21.5	34	4	10	39	2.7
4	LiOH	5	21.5	14	8	6	64	1.6
5	Triton® B, KOH	1, 4	17.5	2	27	14	48	4.2

The ideal amount of 4.5 equiv of Triton® B was necessary as the base for cyclization, saponification of the ester, and to quench the bromination reagent and by-products. The reaction was run at 0 °C for 12 hours then warmed to 20 °C until the bromo-acid intermediate **60** was consumed. The cyclization was performed at these temperatures to minimize the formation of the diol impurity **61** which was formed at higher levels at warmer temperatures, while also minimizing cycle time by ensuring complete conversion at the warmer temperature.

Cyclization of Diastereomeric Impurities.

In order to develop a control strategy that ensured the chiral purity of macrocycle **3**, impurity fate and purge studies were conducted with the potential stereoisomers of the chiral components **38**, **40**, and **46**. These fate and purge studies revealed that the potential stereoisomers were completely cleared in the isolation of macrocycle **3**, or in earlier isolated intermediates (**13**, **49**, or **31**). Several of the potential stereoisomers of allylic bromide **12** were carried through the cyclization reaction, as outlined in Scheme 14 for the enantiomer of hydroxy proline **46**. The

allylic bromide stereoisomer derived from **ent 46** resulted in only 36% cyclization to the corresponding macrocycle **bis-epi 3**, with hydrolysis of the allylic bromide being a major side reaction forming 30% of **bis-epi 61**. A low level of cyclization (49%) was also observed for the allylic bromide stereoisomer derived from the carboxylate epimer of hydroxy proline **46**, with hydrolysis of the allylic bromide occurring to the extent of 42%. These results were somewhat surprising given that allylic bromide **12** undergoes 86% cyclization to macrocycle **3**, as shown in entry 1 of Table 5. Based on these observations, the conformation of allylic bromide **12** facilitates cyclization to the macrocycle at a significantly faster rate than hydrolysis, in contrast to the other allylic bromide stereoisomers.[25]

Scheme 14: Cyclization of an Allylic Bromide Stereoisomer

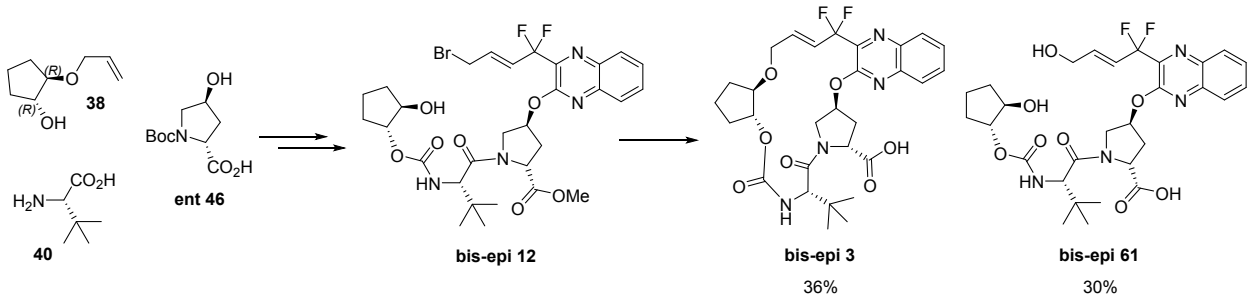

Reactive Quench of Allylic Bromides

At the end of the reaction, a small amount of bromo-acid **60** remains, along with several other impurities that contain the allylic bromide functional group. As part of the mutagenic impurity control strategy, based on ICH M7 guidance, the allylic bromides were assigned as class 3 unless an Ames test had been performed, and then as Class 2 if the Ames test was positive or Class 5 if the Ames test was negative.[26] In order to develop a control strategy for all the allylic bromides potentially present, a quench using 2-mercaptoethylamine (cysteamine) was used to react with the entire class as shown in Scheme 15 for two allylic bromides. Displacement of the allyl bromide functional group with the thiol results in daughter impurities classified as non-

mutagenic, therefore allowing them to be controlled as ordinary impurities. The development of this method, along with the kinetics underpinning the control of these impurities has been previously described.[27] The 2-mercaptoethylamine hydrochloride salt (2 equiv. relative to remaining allylic bromides) is charged to the reaction solution and reacts with any remaining allylic bromide intermediates or impurities and aids in removal of these impurities in the crystallization. As shown in Figure 4, the reactive quench is very fast with a half-life of less than one minute; a 30 min stir time ensures complete conversion of all the remaining allylic bromides.

Scheme 15: Reactive Quench of Residual Allylic Bromides

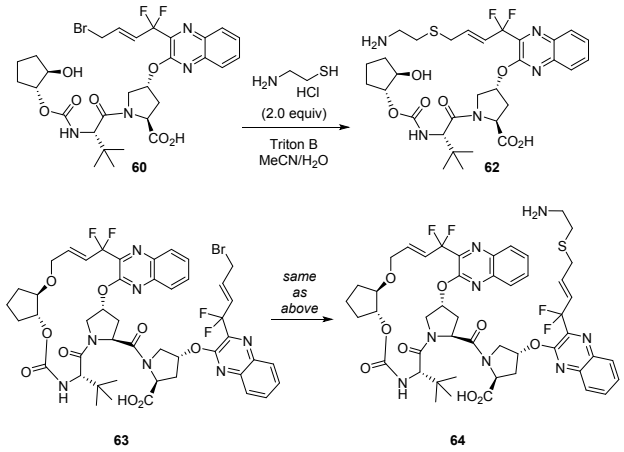

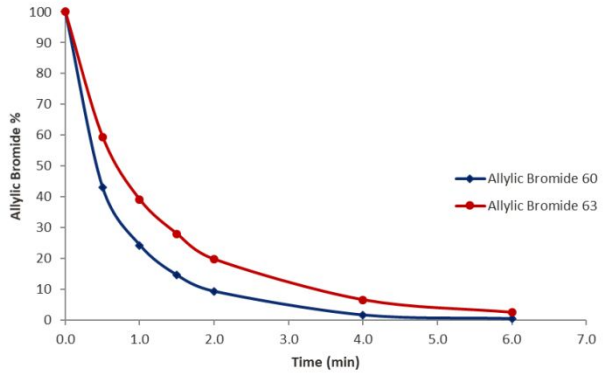

Figure 4. Kinetics for Reactive Quench of Allylic Bromides

Isolation of Macrocycle 3

In the context of the overall synthesis of glecaprevir, the isolation of the macrocycle **3** was a key purification point as this is the final intermediate prior to the formation of the API, so

understanding of impurity rejection was important. An additional challenge was the rejection of the reagents and by-products from the three telescoped steps, including 4.5 equiv. of Triton® B and 1.25 equiv. of PPh_3O.

Initial development of a workup provided purification of the product, although in total the workup required 1 week of processing time per batch. This workup first involved acidification and extraction of the product into toluene to separate the product from most of the Triton® B. The product could then be extracted as the potassium salt into an aqueous layer which allowed for the rejection of the PPh_3O in the toluene layer. The product could then be isolated by acidification and extraction into 2-MeTHF. Two crystallizations, one from 2-MeTHF/water and a second from 2-MeTHF/heptanes, were required to provide macrocycle **3** with the desired quality.

As this route was further evaluated for late-stage development, there were clear advantages if the reaction workup/isolation could be simplified. Improvements to the upstream process provided increased consistency in the starting materials, and allowed for close evaluation of impurity formation, fate and clearance. Critical evaluation of the isolation process showed that the complex workup was needed primarily for rejection of the PPh_3O byproduct of the bromination reaction. We began to consider if a crystallization directly from the cyclization reaction mixture (MeCN/water) would be possible (Figure 5). This would remove many of the unit operations in the previous workup protocol, and would be increasingly streamlined, even if recrystallization was necessary. The solubility of PPh_3O was >200 mg/mL in a 2/1 mixture of MeCN/water. Based on this data, it would be feasible to develop a crystallization process that solubilized the PPh_3O while allowing crystallization of macrocycle **3**.

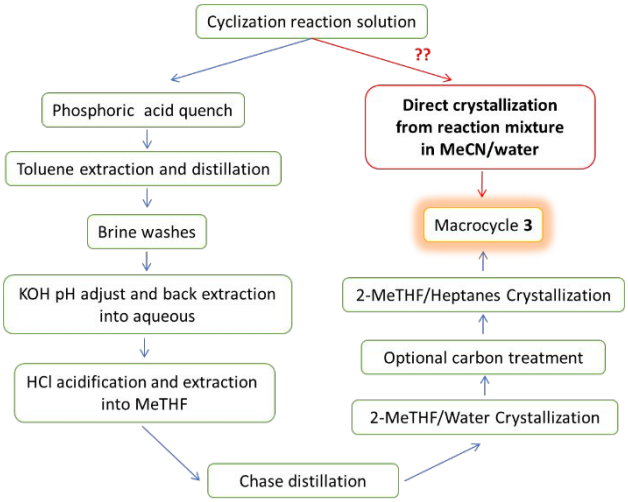

Figure 5: Cyclization Workup Prior to Development of a Direct Crystallization

At the end of the reaction, acidification was necessary to protonate the carboxylic acid. A screen of phosphoric acid, HCl, and formic acid was conducted for the direct crystallization process. In all cases, oiling of PPh_3O was observed; however, with formic acid this oiling was observed near a point of complete desaturation of the product. Macrocycle **3** was known to form a variety of solvates with 2-MeTHF, heptane, MeCN, toluene, and water. The solvates of 2-MeTHF and toluene were favorable due to the improved physical properties of the isolated solid. A screen of crystallization conditions was conducted varying the amount of formic acid, water, and 2-MeTHF or toluene added (Table 6). In the absence of 2-MeTHF or toluene, macrocycle **3** precipitated as a gum (Entry 1). Increasing the amount of 2-MeTHF, formic acid, and water added to the reaction mixture provided the solid 2-MeTHF solvate with complete rejection of the PPh_3O, although at high losses of product (entries 2-4). Addition of more water anti-solvent provided a sticky solid and was not an option to increase recovery. In the cases where toluene was added (entry 5), the toluene solvate was obtained and significantly less product loss was observed (6.6%), however a small amount of PPh_3O was present in the isolated solid.

Interestingly, increasing the amount of formic acid from 1.18 g/g to 2.88 g/g resulted in the same loss with half the amount of PPh_3O in the isolated solid (entry 6).[28] Based on the promise of this screen, the isolation of the toluene solvate of macrocycle **3** was developed further.

Table 6. Initial Screen of Conditions for Direct Crystallization of Macrocycle **3** from MeCN/Water

Entry	pH	Formic Acid (g/g)	Water (g/g)	2-MeTHF (g/g)	Toluene (g/g)	Loss to Liquors	PPh_3O in **3** (HPLC area %)	Form
1	3.74	1.16	11.7	0	0	33.5%	ND	Gum
2	3.74	1.16	11.7	0.45	0	37.0%	0	Solid
3	3.74	1.16	11.7	1.3	0	30.3%	0	Solid
4	2.88	2.92	14.2	1.3	0	27.3%	0	Solid
5	3.74	1.18	14.2	0	0.3	6.6%	3.2%	Solid
6	2.90	2.88	14.2	0	0.3	6.7%	1.6%	Solid

To further explore this crystallization and the key interactions between the parameters of formic acid, water, toluene, and temperature on the loss of product and the residual level of PPh_3O (TPPO) in the isolated solid, a DOE (fractional factorial design with some 2-factor interactions and 3 center points) was used to investigate the design space of the crystallization process. It was also determined that 1.3% of PPh_3O could be rejected in the downstream process. The response from this DOE did not show any secondary interactions over the range of parameters studied. Formic acid had a minor impact on both yield and PPh_3O levels in the range of 2.6-3.2 kg/kg. Both water and toluene showed a disparate influence on the measured outputs, as low water or toluene charges gave lower levels of PPh_3O but increasing the loss of product, while high water or toluene charges gave lower losses but higher PPh_3O levels. Temperature was shown to have a limited impact on PPh_3O levels, but substantially impacted the loss of product, and so a nominal temperature of 10 °C was chosen. This DOE identified final conditions very close to the conditions from the initial screen, with formic acid at 3.0 kg/kg, water at 14.1 kg/kg,

toluene at 0.28 kg/kg (1.26 eq.) and 10 °C final temperature being the preferred conditions for the isolation of the product.

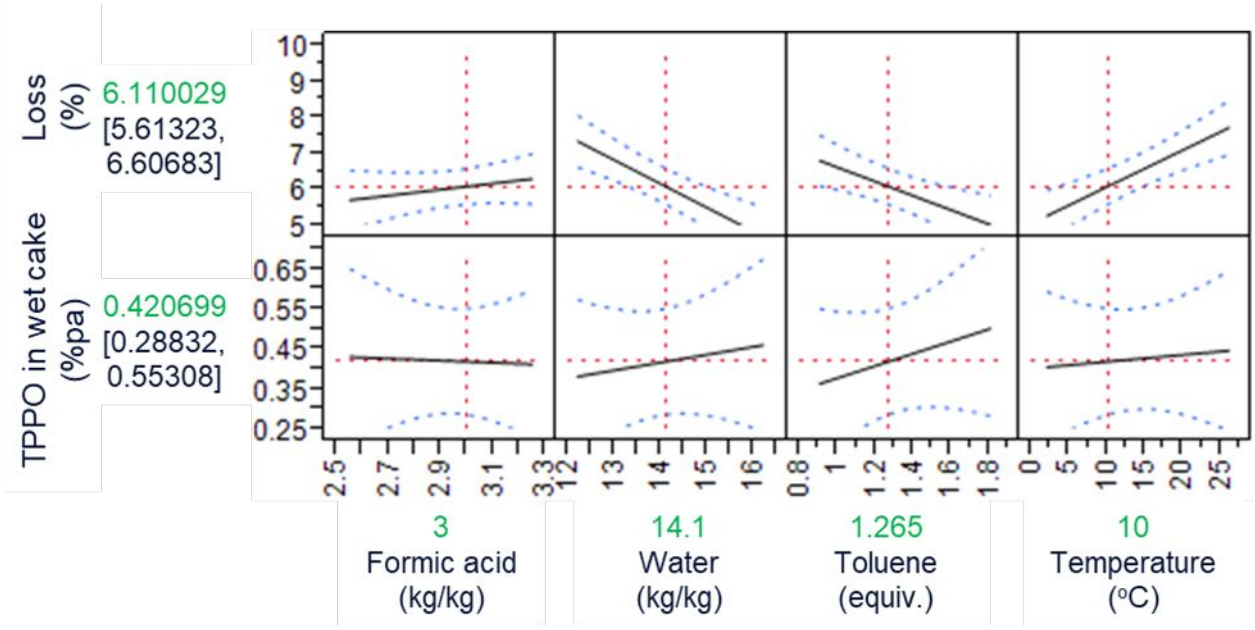

Figure 6: Results of the DOE Study on Macrocycle **3** Crystallization

Based on the solubility data the crystallization process was developed to ensure controlled nucleation and consistent product purity. The reaction was quenched with formic acid and warmed to 45 °C. Toluene was added and the crystallization seeded, water was added slowly to further desaturate followed by cooling to 10 °C. The product was isolated and washed with MeCN/water which further reduced the level of PPh_3O in the isolated product.

Xylene Solvate Increases Overall Yield

During the development of this process a small peak in the HPLC chromatogram of macrocycle **3** was observed at variable levels and was tied to the lot of toluene that was used. This impurity was identified as *p*-xylene, which is a known impurity in toluene. The interesting observation was that the level of *p*-xylene in the product was enriched compared to the amount present in the toluene, from <0.2% to 0.8%. This led to a hypothesis that the *p*-xylene solvate

was favored compared to the toluene solvate and may also lead to lower losses in the crystallization. To test this hypothesis, a series of crystallizations (Table 7) varying the ratio of toluene and *p*-xylene was conducted, and lower loss to the liquors was observed without sacrificing quality of the product when the *p*-xylene level was high. An overall increase in yield of 5% was obtained by simply switching from toluene to *p*-xylene.

Table 7. Study of Toluene and *p*-Xylene Equivalents in Crystallization

Entry	Toluene (equiv)	*p*-Xylene (equiv)	Liquor Conc. of **3** (mg/g)	Loss to Liquors	PPh_3O in **3** (HPLC area %)
1	1.28	0	2.0	9.6%	0
2	0.70	0.53	1.5	7.2%	0
3	0.63	0.63	1.4	6.7%	0
4	0.18	1.08	1.2	5.8%	0
5	0	1.29	0.9	4.3%	0.26

X-ray Crystal Structures

To understand the solubility differences between the toluene and *p*-xylene solvates, the single crystal structures of these solvates were examined. These were further compared with a process-relevant but less stable acetonitrile solvate. Both *p*-xylene and toluene solvate single crystal structures of the macrocycle **3** are isostructural hemi-solvates with a Trigonal P3121 space group. Of note, spiral chains of macrocycle **3** molecules are formed through hydrogen bonding and quinoxaline π-stacking (Figure 7). The acetonitrile solvate exhibits similar hydrogen bonding spiral chain networks but lacks the quinoxaline π-stacking which results in one of the three molecules in the asymmetric unit to be inequivalent to the others. All the solvates examined are labile hydrates with water molecules located in channels, providing rationale for the observed hygroscopicity of macrocycle **3**.

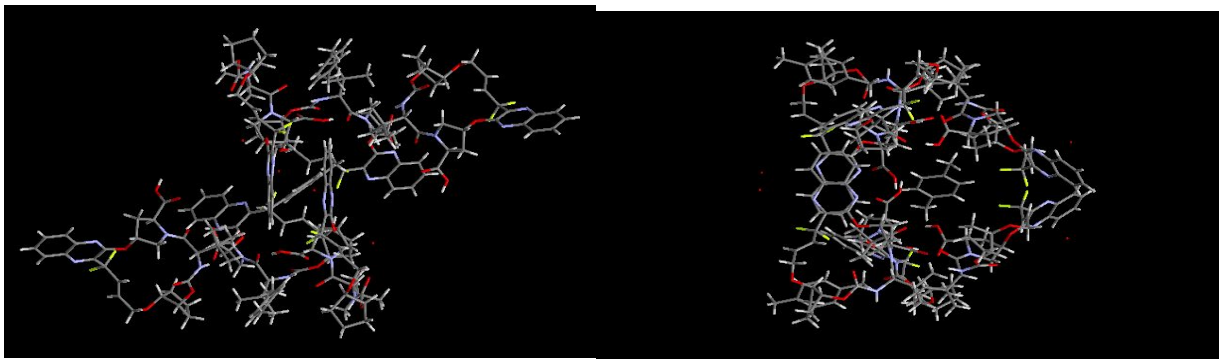

Figure 7: Hydrogen Bonding Spiral and π-stacking in Macrocycle **3** *p*-Xylene Solvate Crystals

The propensity for the macrocycle **3** to form solvates is apparent from these crystal structures. The shape of the macrocycle **3** molecules leaves void spaces that require additional stabilization by solvent (Figure 8). In the toluene and *p*-xylene solvates these void spaces are "pockets" between spiral chains. In the acetonitrile solvate the void spaces consist of both channels and pockets between spiral chains, which can promote facile egress of solvent molecules and explains the relative instability of the acetonitrile solvate.

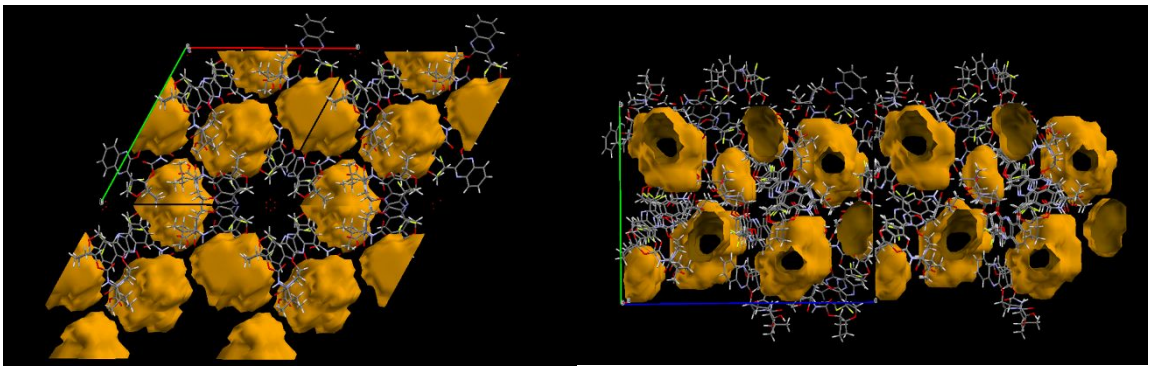

***p*-Xylene solvate** **MeCN solvate**

Figure 8: Calculated "Void" Spaces Occupied by Solvent in Macrocycle **3** Crystals

Further inspection of the toluene and *p*-xylene crystal structures indicates the reason for lower *p*-xylene solubility (Figure 9). In the toluene solvate additional void spaces are observed in the

solvent pocket, whereas these void spaces are filled by the *p*-xylene. The more efficient occupation of these pockets explains the additional stability of the *p*-xylene solvate, which manifests itself as lower solubility in the crystallization.

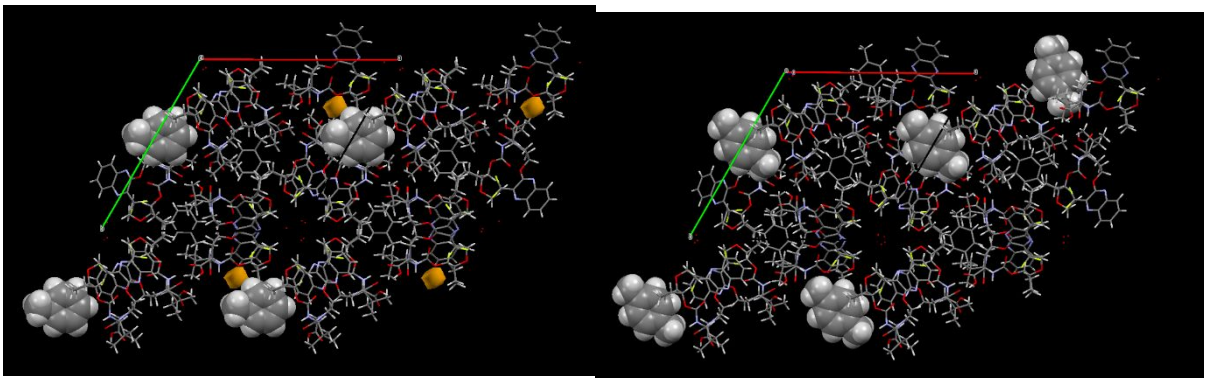

Toluene solvate ***p*-Xylene solvate**

Figure 9: Differences in Void Spaces Between Toluene and *p*-Xylene Solvates of Macrocycle **3**

The three-step, telescoped process with the direct crystallization has been demonstrated on >100 kg scale. This process results in a 77-82% three-step yield and very high purity (Table 8). This robust process to macrocycle **3** was a key impurity control point. Impurities from earlier stages and impurities formed in the telescoped three-step process to macrocycle **3** were well rejected which provides a robust control strategy for the upstream impurities and reduces the burden on downstream purification to ensure consistently high purity API. As an example, the daughter impurities from the 0.5% of *cis* isomer impurity in **31** were rejected below the limit of detection in macrocycle **3**.

Table 8. Performance of Direct Crystallization on Scale

Entry	Batch Size (kg)	Yield from **31** (%)	Purity of **3** (HPLC area %)	PPh_3O in **3** (HPLC area %)
1	96	79	> 99.9	< 0.10
2	194	78	> 99.9	< 0.03
3	169	78	99.7	0.3
4	187	80	> 99.9	< 0.03
5	182	77	> 99.9	< 0.03
6	188	82	> 99.9	< 0.03

Conclusion

An efficient process was developed for synthesis of macrocycle **3**, a penultimate intermediate in the manufacture of glecaprevir. The large-scale route to macrocycle **3** represents a significant improvement over the enabling route as it does not require chromatographic purification and overcomes the scale limitations of the RCM reaction.[2] The application of a Claisen rearrangement to the commercially available ethyl trifluoropyruvate **17** formed the key carbon-carbon bond with the requisite *gem*-difluoromethylene functionality in quinoxaline **32**. A dihydroxylation and carbonate opening facilitated the allylic oxidation with transposition, forming the allylic alcohol **31**. The carbonate opening was found to be exceptionally selective, forming the alkene in a 200:1 *trans:cis* ratio. Upon opening, the carbonate served as a transient protecting group for the allylic alcohol functionality, facilitating the subsequent S_NAr reaction in a two-step, one-pot sequence. The key step in the synthesis was the macrocycle formation through a facile intramolecular etherification of allylic bromide **12**. The final three-step sequence to macrocycle **3** (coupling, bromination, and cyclization) was accomplished in an exceptional 79% overall yield. The identification of solvates with low solubility allowed the crystallization of macrocycle **3** in high purity directly from the reaction mixture, eliminating a complicated

workup. The overall yield to macrocycle **3** was 20% for the lowest yielding sequence through carbamate **13**, a significant improvement over the 15% yield of the enabling route.

Experimental Section

General Information: All reagents and solvents were purchased from commercial vendors and used without further purification. ^{1}H NMR spectra were recorded on either a 400 MHz spectrometer, and chemical shifts (δ) are referenced to either TMS or the NMR solvent. ^{13}C NMR spectra were obtained at 101 MHz and referenced to the NMR solvent. Purity results reported by HPLC and GC analysis are listed in area percent.

HPLC samples were analyzed using an Agilent 1200 system equipped with a UV-DAD detector. Numerous HPLC methods were developed for the analysis of the reactions and products. The HPLC columns were typically an Ascentis Express C8 or C18 column (or equivalent), 10 or 15 cm × 4.6 mm, and 2.7 μm particle size. The mobile phases were acetonitrile and either 0.1% H_3PO_4 or 0.1% $HClO_4$ with a gradient from 10% acetonitrile to 90% acetonitrile over 10 to 15 minutes. LC-MS samples were analyzed using similar methods with the exceptions of using 0.1% formic acid in both the aqueous and the acetonitrile mobile phases, and an ESI detector in positive ion mode.

Analysis by GC-FID was conducted on an Agilent DB-5 column, 30 m × 0.32 mm ID × 0.25 μm film thickness. The injection temperature was 200 °C, the initial column temperature was 50 °C with a 1 min hold followed by a 20 °C/min ramp rate to 240 °C and a 0.5 min hold at 240 °C. The retention times of the compounds analyzed using this method are: **17** at 1.0 min, **41** at 3.6 min, **42** at 3.3 min, and **33** at 3.2 min.

Carbamate 13: The synthesis of **9** was completed as previously described.[2] A solution of **9** (205 kg, 684 mol, 1.0 equiv.) in *i*-PrOAc and heptane was concentrated under vacuum to a

volume of approximately 460 L, and chase distilled with methanol (3 x 370 kg) back to 460 L. To this solution was charged methanol (675 kg), 0.6% aqueous HCl (921 kg), and 10% Pd/C (34.8 kg wet weight). The mixture was heated to 50 °C for 16 h and HPLC analysis showed reaction completion. The reaction was cooled to 20 °C and filtered, and the solids were washed with a mixture of methanol (260 kg) and water (212 kg). The combined filtrates were distilled under vacuum to approximately 1390 L. A solution of 50% NaH_2PO_4 (99 kg) was charged to adjust the pH of the solution to 2.2. The solution was extracted twice with *i*-PrOAc (1575 kg, 471 kg). The combined *i*-PrOAc extracts were distilled under vacuum to a volume of approximately 800 L and then dried by chase distillation with *i*-PrOAc (982 kg total) back to 800 L. The solution was diluted with *i*-PrOAc (137 kg) and then diisopropylamine (40.3 kg, 0.583 equiv.) was added while mixing at a temperature of 25 °C. The crystallization was seeded (343 g) and mixed for 1 h followed by addition of diisopropylamine (33.5 kg, 0.484 equiv.). After mixing for 1 h, heptane (927 kg) was added followed by mixing for 15 h. The solid was isolated, and the cake washed with a mixture of *i*-PrOAc (207 kg) and heptane (289 kg). The wet cake was dried at 35 °C for 10 h and the dry weight of **13** was 214 kg (87% yield from **9**, 99.9% HPLC purity, yield from **38** was 79%). ^{1}H NMR (400 MHz, DMSO-d_6) δ 10.15 – 6.49 (m, 2H), 5.95 (d, J = 8.5 Hz, 1H), 4.60 (dt, J = 6.3, 3.1 Hz, 1H), 3.90 (dt, J = 6.0, 3.4 Hz, 4H), 3.50 (d, J = 8.5 Hz, 1H), 3.22 (hept, J = 6.5 Hz, 2H), 2.01 – 1.86 (m, 1H), 1.78 (ddt, J = 12.3, 9.0, 6.1 Hz, 1H), 1.72 – 1.51 (m, 2H), 1.52 – 1.37 (m, 2H), 1.18 (d, J = 6.4 Hz, 12H), 0.88 (s, 9H). ^{13}C NMR (101 MHz, DMSO) δ 173.29, 155.63, 80.86, 75.18, 63.97, 45.41, 34.11, 31.97, 29.60, 27.12, 20.68, 19.07. HRMS calcd $C_{12}H_{22}NO_5$ $[M+H]^+$: 260.1492, Found 260.1504. Melting point 144-148 °C.

Quinoxaline 43. To a reactor was charged dichloromethane (3.0 L/kg of **17**) followed by pyridine (1.30 equiv) and then by ethyl 3,3,3-trifluoro-2-oxopropanoate **17** (1.00 equiv). The solution was cooled to 0 °C and allyl alcohol (1.05 equiv) was charged while maintaining a temperature of NMT 15 °C. To another reactor was charged dichloromethane (3.0 L/kg of **17**). The temperature was adjusted to 0 °C and thionyl chloride (1.30 equiv) was charged. The hemiketal solution was transferred to the thionyl chloride solution at NMT 15 °C, followed by a rinse of dichloromethane (1 L/kg of **17**). Upon reaction completion, the crude product solution was quenched into a reactor containing 20% potassium phosphate tribasic (NLT 6 L/kg of **17**) while maintaining the temperature below 25 °C and the pH above 6.3. After mixing the layers separated and the organic layer was washed 5% hydrochloric acid (5.0 L/kg of **17**), and then 20% potassium phosphate tribasic (3.0 L/kg of **17**) to obtain a pH of approximately 7. The organic layer was distilled at atmospheric pressure to concentrate and dry the product solution. The yield of **41** was typically 85% with >98% purity as determined by GC analysis.

To a vessel was charged a solution of **41** in DMF (35 to 60 wt%). The solution was sparged with nitrogen to remove oxygen and cooled to 0 °C. To a separate vessel was charged Zn dust (1.30 equiv) and DMF (2.0 L/kg of **41**). The slurry was sparged with nitrogen to remove oxygen to below 50 ppm, and then cooled to 15 °C and chlorotrimethylsilane (0.10 equiv) was added with vigorous mixing of the slurry at NMT 30 °C for approximately 90 minutes. After activation, the zinc slurry was cooled to 0 °C and then charged in portions to the solution of **41** while maintaining the temperature below 15 °C. Upon completion of the addition, the reaction was analyzed by GC for conversion of **41** to **42**. The reaction was filtered through celite (0.25 kg/kg of **41**), rinsing with DMF (1.0 L/kg of **41**) to wash the solids. The solution was heated to 80 °C and analyzed for conversion of **42** to **33**. Upon completion, the reaction was cooled to 0 °C. In a

separate vessel, benzene 1,2-diamine **16** (0.90 equiv) was dissolved in DMF (0.75 L/kg of **41**) and sparged with nitrogen. The solution of **16** was then charged to the reaction maintaining a temperature of NMT 25 °C, rinsing with DMF (0.25 L/kg of **41**) to complete the transfer. The temperature was adjusted to 20 °C. The reaction was analyzed by HPLC for the formation of **43**. The temperature was adjusted to 40 °C and 10% ammonium chloride (9 – 10 L/kg of **41**) was slowly charged. The slurry was cooled to NMT 25 °C, filtered, and the wet cake washed once with a 3:1 water:DMF solution (2 L/kg of **41**) and then twice with water (2 × 3 L/kg of **41**). The wet cake was dried under vacuum at 60 °C. The dried product **43** was recrystallized from toluene (NLT 3.5 L/kg of **43**) and heptanes (15 L/kg of **43**). The wet cake was dried under vacuum at 60 °C. The yield of **43** was typically 65% from **41** with >99.8% purity by HPLC. ^{1}H NMR (400 MHz, DMSO-d_6) δ 12.79 (s, 1H), 7.85 (dd, J = 8.4, 1.4 Hz, 1H), 7.63 (ddd, J = 8.6, 7.2, 1.4 Hz, 1H), 7.39 – 7.32 (m, 2H), 5.77 (ddt, J = 17.2, 10.2, 7.1 Hz, 1H), 5.24 (dq, J = 17.1, 1.6 Hz, 1H), 5.18 (ddt, J = 10.2, 1.9, 1.0 Hz, 1H), 3.25 (tdt, J = 17.3, 7.1, 1.3 Hz, 2H). ^{13}C NMR (101 MHz, DMSO-d_6) δ 151.84, 149.71 (t, J = 25.4 Hz), 132.47, 131.75, 129.75, 129.02, 128.30 (t, J = 5.1 Hz), 123.38, 120.58, 118.76 (t, J = 243.5 Hz), 115.14, 39.14 (t, J = 24.5 Hz). HRMS calcd $C_{12}H_{11}F_2N_2O$ $[M+H]^+$: 237.0834, Found 237.0829. Melting point 145-147 °C.

Quinoxaline 32: To a reactor was charged quinoxaline **43** (60.9 kg, 97% potency, 250 mol, 1.0 equiv.), toluene (318 kg), DMF (21.0 kg, 287 mol, 1.15 equiv.), and $POCl_3$ (45.6 kg, 294 mol, 1.18 equiv.). The mixture was heated to 50 °C for 6 h and then cooled to 20 °C and mixed for 7.5 h and HPLC analysis confirmed reaction completion. The reaction was cooled to 0 °C and then quenched with cold water (239 kg). The temperature was adjusted to 20 °C and the layers separated. The toluene layer was washed successively with water (302 kg), 10% Na_2HPO_4 (298 kg), and 25% brine (297 kg). The solution was then filtered through a pad of magnesium sulfate

(50 kg), rinsing with toluene (130 kg). The filtrate was concentrated under vacuum to a volume of approximately 100 L, diluted with IPA (163 kg), concentrated to a volume of 200 L, and then chased with IPA (304 kg) maintaining the volume at 200 L. The mixture was diluted with IPA (130 kg) and the temperature adjusted to 40 °C. An aliquot of the solution (10 kg) was removed and allowed to cool to form a seed slurry. The bulk solution was cooled to 28 °C and the seed slurry was charged. After aging for 1 h, the slurry was slowly cooled to 20 °C and mixed for 2 h. The slurry was diluted with water (679 kg) over 2 h and then aged for 8 h. The slurry was filtered, and the cake washed with a mixture of IPA (22 kg) and water (44 kg). The cake was dried under vacuum at a temperature of 30 °C. The isolated weight of quinoxaline **32** was 61.2 kg (98.4% potency, 236 mol, 95% yield). ^{1}H NMR (400 MHz, Chloroform-*d*) δ 8.13 (dd, *J* = 8.3, 1.6 Hz, 1H), 8.05 – 8.01 (m, 1H), 7.89 – 7.78 (m, 2H), 5.95 (ddt, *J* = 17.2, 10.2, 7.0 Hz, 1H), 5.31 (dq, *J* = 17.2, 1.5 Hz, 1H), 5.26 – 5.22 (m, 1H), 3.33 (tdt, *J* = 16.8, 7.0, 1.3 Hz, 2H). ^{13}C NMR (101 MHz, Chloroform-*d*) δ 145.94 (t, *J* = 30.7 Hz), 144.45, 141.99, 138.93, 132.62, 131.01, 129.65, 128.60 (td, *J* = 5.1, 2.0 Hz), 128.26, 121.30, 119.94 (t, *J* = 244.2 Hz), 40.20 (t, *J* = 24.5 Hz). HRMS calcd $C_{13}H_{10}ClF_2N_2$ $[M+H]^+$: 255.0495, Found 255.0483. Melting point 61-62 °C.

Ether 47: To a reactor was charged NaH (60% dispersion in mineral oil in THF soluble bags, 40. kg, 1000 mol, 2.2 equiv.) and THF (390 kg). To a separate reactor was charged hydroxyproline **46** (115 kg, 497 mol, 1.1 equiv) and THF (351 kg) and this solution was slowly charged to the NaH slurry maintaining the temperature below 25 °C, rinsing with THF (50 kg) to complete the transfer. To a separate reactor was charged quinoxaline **32** (114.4 kg, 449 mol, 1.0 equiv.) and THF (216 kg). Both reactors were adjusted to 5 °C. The quinoxaline **32** solution was charged to the hydroxyproline **46** slurry maintaining the temperature at NMT 10 °C, rinsing with

THF (51 kg) to complete the transfer. The reaction was adjusted to 20 °C and mixed for 24 h until HPLC analysis confirmed reaction completion. The reaction was cooled to NMT 10 °C and then quenched with cold water (720 kg) maintaining the temperature below 25 °C. The mixture was extracted with heptanes (540 kg) and the aqueous layer was then re-extracted with a mixture of MTBE (396 kg) and heptanes (183 kg). The aqueous layer was extracted with MTBE (451 kg) and the pH lowered to 3 with 85% H_3PO_4 (67.6 kg). The MTBE layer was washed with water (2 x 230 kg). The solution was dried by distillation under vacuum (approximately 200 mm) at a constant volume of approximately 850 L by charging MTBE (911 kg). The dried solution was passed through an AKS6 carbon filter cartridge (~ 4 wt% loading relative to **32**) rinsing with MTBE (82 kg). The filtered solution was concentrated under vacuum to 790 L. The temperature was adjusted to 45 °C and diisopropylamine (45.5 kg, 449 mol, 1.0 equiv.) was charged. The solution was warmed to 55 °C followed by the addition of heptanes (680 kg). The crystallization was seeded with **47** (20 kg) slurried in heptanes (100 kg), followed by a rinse with heptanes (70 kg) to complete the transfer. The slurry was mixed for 1 hour followed by cooling to 20 °C. The slurry was filtered, and the cake washed with a mixture of heptanes (208 kg) and MTBE (113 kg). The wet cake was dried under vacuum at 45 °C for an isolated yield of 90% (243.1 kg, net 223.1 kg minus seed, 98.4% purity by HPLC). ^{1}H NMR (400 MHz, Methanol-d_4) δ 8.04 (dd, J = 8.3, 1.1 Hz, 1H), 7.86 (dd, J = 8.4, 1.1 Hz, 1H), 7.79 (ddd, J = 8.4, 6.9, 1.5 Hz, 1H), 7.66 (ddd, J = 8.4, 6.9, 1.5 Hz, 1H), 5.94 – 5.74 (m, 2H), 5.22 (d, J = 17.2 Hz, 1H), 5.15 (d, J = 10.2 Hz, 1H), 4.37 (dd, J = 8.7, 7.5 Hz, 1H), 3.98 – 3.77 (m, 2H), 3.45 (hept, J = 6.5 Hz, 2H), 3.29 – 3.13 (m, 2H), 2.72 – 2.59 (m, 1H), 2.34 (ddd, J = 13.8, 9.0, 4.7 Hz, 1H), 1.46 (s, 9H), 1.32 (d, J = 6.5 Hz, 12H). Note that rotational isomers caused doubling of some ^{13}C signals. ^{13}C NMR (101 MHz, Methanol-d_4) δ 179.80, 156.66, 154.91, 142.40 (t, J = 29.0 Hz), 142.05, 138.33, 132.87, 130.23,

129.96, 128.79, 127.98, 121.39, 120.69 (t, J = 245.3 Hz), 81.24, 76.51, 62.04, 53.30, 48.30 (d, J = 1.6 Hz), 41.40 (t, J = 25.3 Hz), 38.02, 28.74, 19.37. HRMS calcd $C_{22}H_{26}F_2N_3O_5$ $[M+H]^+$: 450.1835, Found 450.1841. Melting point 132-137 °C.

Allylic Alcohol 49: To a reactor was charged ether **47** (134.4 kg, 96.4% potency, 235 mol, 1.0 equiv.) and EtOAc (510 kg) and the mixture washed with twice with 1 M HCl (331 kg, 167 kg), and 25% brine (254 kg). The EtOAc solution was concentrated under vacuum to a volume of approximately 300 L and chased with MeCN (894 kg) maintaining the volume at 300 L. The solution was diluted with MeCN (591 kg), filtered, rinsing with MeCN (80 kg), and then concentrated under vacuum to 300 L. The MeCN solution was then transferred to a reactor containing water (600 kg) and $NaHCO_3$ (187 kg, 2230 mol, 9.5 equiv.), rinsing with MeCN (30 kg) to complete the transfer. The mixture was diluted with water (503 kg) and cooled to 0 °C. Trifluoroacetone (50.0 kg, 446 mol, 1.9 equiv.) was charged followed by addition of Oxone® (343 kg, 1120 mol, 4.7 equiv.) over approximately 7 h. After mixing for approximately 1.8 h at 0 °C, HPLC analysis confirmed reaction completion. The reaction mixture was filtered through a filter pot to collect the solids, and solids were rinsed with a cold solution of EtOAc (901 kg) and water (18 kg), A 25% sodium bisulfite solution (321 kg) was added to the filtrate and the pH was adjusted to 6.2 charging 20% citric acid (70 kg), maintaining the temperature at approximately 5 °C throughout the workup. The aqueous layer was separated and re-extracted with EtOAc (592 kg) and the EtOAc extracts were combined, rinsing with EtOAc (35 kg) to complete the transfer. The EtOAc solution was washed with 25% brine (501 kg) and then added 50% NaOH (17.8 kg, 223 mol, 0.95 equiv.). The solution was concentrated under vacuum to a volume of approximately 450 L, chasing with toluene. The solution was filtered, rinsing with

toluene. The final toluene solution (659.5 kg) assayed for a 72% yield of the epoxide **48** (82.6 kg, 170 mol).

The toluene solution of epoxide **48** (82.6 kg, 170 mol, 1.0 equiv.) was cooled to -13 °C, and then a toluene solution of potassium *t*-amylate (25%, 223.3 kg, 442 mol, 2.6 equiv.), also at -13 °C, was charged over approximately 30 minutes maintaining the temperature below -5 °C. A sample after 5 min showed reaction completion by HPLC analysis. The reaction was quenched with MeOH (33 kg) and then a solution of DMEDA (44.3 kg, 503 mol, 3.0 equiv.) and H_3PO_4 (85%, 28.8 kg, 250 mol, 1.5 equiv.) in water (158 kg). The reaction was warmed to 20 °C and mixed for 23 h. The reaction was diluted with water (158 kg) and mixed and the layers separated, and the toluene layer was re-extracted with water (80 kg). The combined aqueous extracts were charged to a reactor containing IPAc (482 kg), MeOH (169 kg) and 20.8% H_3PO_4 (613 kg) and then mixed at 25 °C for 1 h, settled and the layers separated. The IPAc solution was then washed with 8.6% H_3PO_4 (417 kg), 5% brine (415 kg), and then water (400 kg). The solution was warmed to 40 °C and passed through an AKS1 carbon filter (7% loading relative to **48**) and an AKS6 carbon filter (3.5% loading relative to **48**), rinsing with IPAc (176 kg). The filtrate was combined with another batch for crystallization and the combined starting amount of **48** was 356 mol. The combined IPAc solutions were concentrated under vacuum to 700 L, diluted with IPAc (150 kg), and concentrated to 750 L. Benzhydrylamine (53.4 kg, 291 mol, 0.81 equiv.) was added and the solution heated to 50 °C, seeded (1.5 kg) and aged for 1 h. The slurry was cooled to -5 °C over 3 h and then aged for 12 h. The slurry was filtered, and the cake washed with IPAc (500 kg) in portions. The wet cake was dried in a vacuum oven at 45 °C for 24 h. The dry weight of **49** was 152.6 kg (96% potency, 92.2% purity, 7.2% *cis* isomer impurity, 226 mol) for a 63% yield.

Cyclic Carbonate 50: To a reactor was charged quinoxaline **32** (230.0 kg, 98.3% potency, 888 mol, 1.0 equiv.), potassium osmate dihydrate (506 g, 1.37 mol, 0.0015 eq) and EtOAc (704 kg). To this mixture was added 50% aqueous NMO (241.5 kg, 1031 mol, 1.16 equiv.) and the mixture heated to 40 °C. After 22 h the reaction was complete by HPLC analysis and was cooled to 20 °C. The reaction was quenched with 15% sodium sulfite (840 kg), diluted with EtOAc (704 kg) and mixed for 2 h. The layers were separated and the EtOAc layer was washed with 10% brine (831 kg), 13% H_3PO_4 (734 kg), and 10% brine (831 kg). The EtOAc solution was concentrated under vacuum to a volume of approximately 575 L and then chased with MeCN (3 x 362 kg) back to volume. The mixture was warmed to 40 °C to form a solution, and then a solution of CDI (227.7 kg, 1404 mol, 1.58 equiv.) in MeCN (2550 kg) was slowly charged. After 1 h the reaction was complete by HPLC analysis, was cooled and then concentrated under vacuum to a volume of approximately 1035 L. The mixture was warmed to form a solution and then cooled to 40 °C and then water (3082 kg) was added while maintaining the temperature at 40 °C and the product crystallized. The mixture was cooled to 22 °C and the product isolated, washing the cake in portions with a solution of MeCN (184 kg) and water (739 kg). The wet cake was dried at 40 °C under vacuum to yield the cyclic carbonate **50** (252.1 kg, 99.8% potency, 801 mol, 90% yield). ^{1}H NMR (400 MHz, DMSO-d_6) δ 8.20 (dd, J = 8.2, 1.4 Hz, 1H), 8.12 (dd, J = 7.9, 1.6 Hz, 1H), 8.04 (ddd, J = 8.4, 6.9, 1.7 Hz, 1H), 7.99 (ddd, J = 8.4, 7.0, 1.7 Hz, 1H), 5.21 (qd, J = 7.7, 4.9 Hz, 1H), 4.71 (t, J = 8.2 Hz, 1H), 4.38 (t, J = 8.1 Hz, 1H), 3.30 – 3.07 (m, 2H). ^{13}C NMR (101 MHz, DMSO-d_6) δ 154.46, 144.36 (t, J = 29.7 Hz), 143.09, 141.47, 138.17, 133.44, 131.78, 129.27, 127.83, 119.69 (t, J = 244.1 Hz), 71.74 (t, J = 4.3 Hz), 69.26, 38.58 (t, J = 23.5 Hz). HRMS calcd $C_{13}H_{10}ClF_2N_2O_3$ $[M+H]^+$: 315.0343, Found 315.0355. Melting point 131-133 °C.

Allylic Alcohol 49: To a reactor was charged cyclic carbonate **50** (75.0 kg, 99.2% potency, 236 mol, 1.0 equiv.) and THF (551 kg) and the solution was cooled to –10 °C. To another reactor was charged hydroxyproline **46** (64.4 kg, 99% potency, 276 mol, 1.17 equiv.) and THF (551 kg) followed by solid potassium *tert*-butoxide (61.4 kg, 547 mol, 2.3 equiv.) in portions. Water was then added to the slurry (2.0 kg, 110 mol, 0.47 equiv.) and was mixed at high agitation at 20 °C. To a third reactor was charged a 0.98 M solution of NaHMDS in THF (253 L, 248 mol, 1.05 equiv.) and the solution cooled below 5 °C. The NaHMDS solution was transferred to the reactor containing the solution of **50** while maintaining the temperature below 0 °C. The reaction was mixed at –5 °C and analysis by HPLC confirmed complete conversion to **51**. The slurry of the hydroxyproline **46** was transferred to the reactor containing **51** while maintaining the temperature below 0 °C, followed by a rinse with THF (50 kg) to complete the transfer. The reaction was mixed at –5 °C for approximately 1 h and HPLC analysis confirmed consumption of **51**. The reaction was quenched with water (202 kg) and then warmed to 20 °C, settled, and the lower layer was separated. The upper layer was distilled under vacuum to a volume of approximately 375 L. The solution was diluted with *i*-PrOAc (320 kg) and water (600 kg) and after mixing the aqueous (product containing) layer was separated. The aqueous layer was re-extracted with *i*-PrOAc (320 kg). The aqueous layer was diluted with *i*-PrOAc (375 kg) and the pH adjusted to 3.0 ± 0.5 with addition of 85% H_3PO_4 and the layers were separated. The aqueous layer was re-extracted with *i*-PrOAc (375 kg) and the *i*-PrOAc extracts were combined. The organic layer was washed three times with 10% sodium phosphate monobasic (3 x 475 kg) and then with water (300 kg). The *i*-PrOAc solution was heated to 45 °C and passed through AKS1 carbon filters (5.6 kg of carbon). The reactor and filters were rinsed with *i*-PrOAc (185 kg) and combined with the filtrate. The *i*-PrOAc solution was concentrated to a target volume of 600 L,

and then a constant volume distillation was performed to dry the solution, charging *i*-PrOAc while maintaining the volume of approximately 600 L. The solution was diluted with *i*-PrOAc to a target volume of 800 L. The mixture was heated to 55 °C and then benzhydrylamine (19.3 kg, 0.45 equiv.) was charged to the solution. The solution was seeded with a slurry of **49** (1.0 kg) in *i*-PrOAc (3 kg), rinsing with *i*-PrOAc (1.5 kg). The mixture stirred at 55 °C until a seed bed was formed. A second portion of benzhydrylamine (19.7 kg, 0.45 equiv.) was charged slowly and the mixture was stirred at 55 °C for approximately 1 h. The crystallization slurry was slowly cooled to 0 °C, and then mixed at 0 °C for NLT 4 h. The slurry was filtered and washed with cold *i*-PrOAc (0 °C) in 3 approximately equal portions (3 × 120 kg). The wet cake was blown dry with nitrogen and then dried under vacuum at 45 °C with a nitrogen sweep. The isolated yield of **49** was 68.1% (107.7 kg adjusted for seed charge, 98.5% purity, 69.6% free acid potency). Rotational isomers observed in the NMR spectra. ^{1}H NMR (400 MHz, Methanol-d_4) δ 8.02 (d, J = 8.3 Hz, 1H), 7.86 – 7.78 (m, 1H), 7.75 (ddt, J = 8.3, 6.9, 1.7 Hz, 1H), 7.62 (ddd, J = 8.3, 6.9, 1.5 Hz, 1H), 7.47 – 7.35 (m, 8H), 7.35 – 7.28 (m, 2H), 6.44 – 6.34 (m, 1H), 6.34 – 6.21 (m, 1H), 5.74 (dp, J = 4.3, 2.0 Hz, 1H), 5.62 (s, 1H), 4.31 (t, J = 8.2 Hz, 1H), 4.27 – 4.16 (m, 2H), 3.94 – 3.75 (m, 2H), 2.64 – 2.51 (m, 1H), 2.32 – 2.17 (m, 1H), 1.47 (s, 9H). ^{13}C NMR (101 MHz, Methanol-d_4) δ 179.82, 156.62, 154.74, 142.58 (t, J = 30.1 Hz), 141.99, 139.21, 138.54 (t, J = 8.3 Hz), 138.29, 132.74, 130.10, 129.69, 128.74, 128.34, 127.90, 123.38 (td, J = 26.5, 6.4 Hz), 117.99 (t, J = 241.7 Hz), 111.98, 81.39, 76.32, 61.86, 61.38, 59.30, 53.21, 37.93, 28.73. HRMS calcd $C_{22}H_{26}F_2N_3O_6$ $[M+H]^+$: 466.1784, Found 466.1786. Melting point 144 °C.

Allylic Alcohol 31: To a reactor was charged allylic alcohol **49** (110.0 kg, net 76.6 kg free acid, 164 mol, 1.0 equiv.) and CPME (516 kg) and the mixture washed twice with 5% H_3PO_4 (2 x 450 kg) and then water (400 kg). The CPME solution was concentrated to a volume of

approximately 180 L and then diluted with MeOH (255 kg). The solution was cooled to approximately - 10 °C and then added $SOCl_2$ (39.6 kg, 333 mol, 2.0 equiv.). The solution was warmed to 20 °C and mixed for 14 h and HPLC analysis confirmed reaction completion. The reaction was quenched with water (1.8 kg) and mixed for 1 h. The reaction was diluted with CPME (275 kg), concentrated under vacuum to a volume of approximately 390 L, and then diluted with CPME (137 kg). The mixture was concentrated under vacuum to a volume of approximately 500 L and chased with CPME (138 kg) while maintaining a constant volume. The slurry was mixed at 20 °C for 7 h and then filtered and the cake washed with CPME (231 kg). The solid was dried under vacuum at 35 °C and the dry weight was 65.6 kg (96.0% purity by HPLC, 99.4% potency, 157 mol) for a yield of 95%. ^{1}H NMR (400 MHz, Methanol-d_4) δ 8.07 (ddd, J = 8.3, 1.5, 0.6 Hz, 1H), 7.89 (ddd, J = 8.4, 1.5, 0.6 Hz, 1H), 7.82 (ddd, J = 8.4, 6.9, 1.5 Hz, 1H), 7.71 (ddd, J = 8.4, 6.9, 1.5 Hz, 1H), 6.47 – 6.33 (m, 2H), 6.01 (tt, J = 5.0, 1.7 Hz, 1H), 4.74 (dd, J = 11.2, 7.2 Hz, 1H), 4.28 – 4.22 (m, 2H), 4.04 (dd, J = 13.6, 5.0 Hz, 1H), 3.91 (s, 3H), 3.78 (dt, J = 13.6, 1.5 Hz, 1H), 2.84 (ddt, J = 14.5, 7.2, 1.6 Hz, 1H), 2.67 (ddd, J = 14.5, 11.3, 5.0 Hz, 1H). ^{13}C NMR (101 MHz, Methanol-d_4) δ 169.45, 154.13, 142.34 (t, J = 30.9 Hz), 141.67, 138.69, 138.30 (t, J = 8.3 Hz), 133.11, 130.26, 129.34, 128.04, 123.78 (t, J = 26.3 Hz), 118.08 (t, J = 241.0 Hz), 76.29, 61.81, 60.12, 54.13 (d, J = 3.3 Hz), 52.35, 35.76. HRMS calcd $C_{18}H_{20}F_2N_3O_4$ $[M+H]^+$: 380.1416, Found 380.1423. Melting point 163-170 °C.

Macrocycle 3: To a solution of **31** (1.0 equiv) in DMA (2.3 kg/kg)[28] was charged DIPEA (3.2 equiv). The mixture cooled to NMT 0 °C and then TMSCl (1.35 equiv) was added and mixed at 10 °C. To another reactor was charged HATU (1.05 equiv.) and DMA (0.93 kg/kg), and then a solution of **13** (1.06 equiv) in DMA (1.4 kg/kg) was added, rinsing with DMA (0.3 kg/kg). The activated acid solution was transferred to the reactor containing **31**, rinsing with DMA (0.3

kg/kg). The reaction was monitored by HPLC for consumption of **31**. The reaction was diluted with toluene (8.8 kg/kg) and quenched with a solution of DMAP (0.05 equiv) in water (15.3 kg/kg). The layers were separated, and the aqueous layer re-extracted with toluene (5.4 kg/kg). The combined toluene extracts were washed with water (9.9 kg/kg), 5% sodium bicarbonate (9.9 kg/kg), and water (9.9 kg/kg). The toluene solution was concentrated under vacuum and solvent switched to acetonitrile. The yield of diol **59** was typically ~ 100% and was used directly in the next steps. An aliquot was purified by chromatography for characterization. ^{1}H NMR (400 MHz, Chloroform-*d*) δ 8.10 (d, *J* = 8.2 Hz, 1H), 7.84 (d, *J* = 8.3 Hz, 1H), 7.73 (t, *J* = 7.6 Hz, 1H), 7.62 (t, *J* = 7.6 Hz, 1H), 6.45 – 6.26 (m, 1H), 6.24 – 6.06 (m, 1H), 5.84 (d, *J* = 4.0 Hz, 1H), 5.48 (d, *J* = 9.4 Hz, 1H), 4.88 – 4.59 (m, 1H), 4.48 – 4.32 (m, 2H), 4.32 – 4.15 (m, 2H), 4.13 (d, *J* = 9.4 Hz, 1H), 4.00 – 3.87 (m, 3H), 3.74 (s, 3H), 3.63 (d, *J* = 2.7 Hz, 1H), 2.74 (dd, *J* = 14.1, 7.8 Hz, 1H), 2.29 (ddd, *J* = 14.0, 9.8, 4.3 Hz, 1H), 1.87 (dq, *J* = 14.4, 7.4 Hz, 2H), 1.78 – 1.34 (m, 4H), 1.01 (s, 9H). ^{13}C NMR (101 MHz, $CDCl_3$) δ 171.98, 171.74, 156.84, 152.99, 141.47 (dd, *J* = 31.4, 27.8 Hz), 140.74, 137.61 (t, *J* = 8.0 Hz), 137.52, 131.62, 129.58, 127.85, 126.96, 122.37 (t, *J* = 26.3 Hz), 116.28 (dd, *J* = 244.4, 240.9 Hz), 83.55, 77.15, 75.11, 61.38, 59.44, 57.96, 53.55, 52.50, 35.31, 34.84, 31.87, 29.88, 26.33, 21.29. HRMS calcd $C_{30}H_{39}F_2N_4O_8$ $[M+H]^+$: 621.2730, Found 621.2704.

A solution of triphenylphosphine (1.25 equiv) in acetonitrile (7.9 kg/kg) was cooled below -5 °C and then bromine (1.27 equiv) was charged and the slurry mixed at -5 °C. The solution of diol **59** (1.0 equiv) was slowly added, rinsing with acetonitrile (0.3 kg/kg). The reaction was mixed at -10 °C for approximately 1 h and then transferred into a reactor containing water (6.7 kg/kg) and 40% aqueous $BnMe_3NOH$ (4.5 equiv) at 0 °C. The reaction was mixed for approximately 20 h and then warmed to 20 °C, mixing until HPLC analysis confirmed reaction completion. The

reaction was quenched with cysteamine HCl (0.11 equiv) and mixed at 23 °C for at least 30 min. The solution was diluted with acetonitrile as needed to achieve the target volume and then warmed to 45 °C and formic acid (3.0 kg/kg) was added. A charge of *p*-xylene (~ 1 equiv) was added followed by seed crystals of **3** (0.01 kg/kg). Water (14.1 kg/kg) was then added slowly. The slurry was aged and then slowly cooled to 10 °C, filtered, and the cake was washed in portions with a mixture of acetonitrile (2.5 kg/kg) and water (5 kg/kg). The wet cake was dried under vacuum at approximately 40 °C. The yield of macrocycle **3** ranged from 77 to 82% from **31**. Spectral data was identical to that previously reported in the literature, with the exception of residual solvents.[2]

AUTHOR INFORMATION

Corresponding Author

* E-mail: russell.cink@abbvie.com

SUPPORTING INFORMATION

Computational methods: all DFT calculations were performed using Jaguar; NMR spectra for compounds **13**, **31**, **32**, **43**, **47**, **49**, **50**, **59**; crystal structure data for compound **3**.

DISCLOSURES

AbbVie and Enanta sponsored and funded the study, contributed to the design, participated in the collection, analysis, and interpretation of data, and in writing, reviewing, and approval of the final publication. All authors are or were employees of AbbVie and may own AbbVie stock.

Haojuan Wei is currently an employee of STA Pharmaceutical. Chen Ding is currently an employee of Alnylam Pharmaceuticals, Inc.

ACKNOWLEDGMENTS

The authors would like to thank Steven J. Wittenberger, Seble Wagaw, Dale Kempf, Keith McDaniel, and Clifford Mitchell for helpful discussions, Linjie Han for conducting the HRMS analysis, Robert W. Miller for analytical support, and Richard Bishop and Jianzhang Mei for experimental support. All contributors are or were employees AbbVie when contributions were provided.

REFERENCES

[1] Zeuzem, S.; Foster, G. R.; Wang, S.; Asatryan, A.; Gane, E.; Feld, J. J.; Asselah, T.; Bourlière, M.; Ruane, P. J.; Wedemeyer, H.; Pol, S.; Flisiak, R.; Poordad, F.; Chuang, W.-L.; Stedman, C. A.; Flamm, S.; Kwo, P.; Dore, G. J.; Sepulveda‐Arzola, G.; Roberts, S. K.; Soto‐Malave, R.; Kaita, K.; Puoti, M.; Vierling, J.; Tam, E.; Vargas, H. E.; Bruck, R.; Fuster, F.; Paik, S.-W.; Felizarta, F.; Kort, J.; Fu, B.; Liu, R.; Ng, T. I.; Pilot‐Matias, T.; Lin, C.-W.; Trinh, R.; Mensa, F. J. Glecaprevir–Pibrentasvir for 8 or 12 Weeks in HCV Genotype 1 or 3 Infection *N. Engl. J. Med.* **2018**, *378*, 354.

[2] Cink, R. D.; Lukin, K. A.; Bishop, R. D.; Zhao, G.; Pelc, M. P.; Towne, T. B.; Gates, B. D.; Ravn, M. M.; Hill, D. R.; Ding, C.; Cullen, S. C.; Mei, J.; Leanna, M. R.; Henle, J.; Napolitano, J. G.; Nere, N. K.; Chen, S.; Sheikh, A; Kallemeyn, J. M. Development of the Enabling Route for Glecaprevir via Ring-Closing Metathesis. *Org. Process Res. Dev.* **2020**, *24*, 183.

[3] (a) Cink, R. D.; Lukin, K. A.; Leanna, M. R.; Pelc, M. J.; Towne, T. B.; Welch, D. S.; Engstrom, K. E.; Ravn, M. M.; Bishop, R. D.; Zhao, G.; Mei, J.; Kallemeyn, J. M.; Hill, D. R.; Abrahamson, M. J.; Morrill, W. H. Synthetic Route to Anti-Viral Agents. US 9,809,576 B1, 2017 (b) Abrahamson, M. J.; Kielbus, A. B.; Riordan, W. T.; Hill, D. R.; Chemburkar, S. R.; Reddy, R. E.; Towne, T. B.; Mei, J.; Brown, G. J.; Mix, S. Enzymatic Process for the Preparation of (1S,2R)-2-(Difluoromethyl)-1-(propoxycarbonyl)cyclopropanecarboxylic Acid. US 10,316,338 B1 2019 (c) Lukin, K. A.; Mei, J.; Hill, D. R.; Abrahamson, M. J. Difluoroalkylcyclopropyl Amino Acids and Esters, and Syntheses Thereof. US 9,809,534 B1 2017 (d) Abrahamson, M. J.; Chemburkar, S. R.; Kielbus, A. B.; Cink, R. D. Enzymatic Processes for the Preparation (±)-2-(Difluoromethyl)-1-(Alkoxycarbonyl)-Cyclopropanecarboxylic Acid and (±)-2-(Vinyl)-1-(Alkoxycarbonyl)-Cyclopropanecarboxylic Acid. WO 2018/144681 A1, 2018; US 10,689,675 B2, 2020.

[4] Following manuscript.

[5] For related examples see (a) Feng, Z.; Xiao, Y.-L.; Zhang, X. Transition-Metal (Cu, Pd, Ni)-Catalyzed Difluoroalkylation via Cross-Coupling with Difluoroalkyl Halides. *Acc. Chem. Res.* **2018**, *51*, 2264. (b) Ge, S.; Chaladaj, W.; Hartwig, J. F. Pd-Catalyzed α-Arylation of α,α-Difluoroketones with Aryl Bromides and Chlorides. A Route to Difluoromethylarenes. *J. Am. Chem. Soc.* **2014**, *136*, 4149. (c) Sumino, S.; Uno, M.; Fukuyama, T.; Ryu, I.; Matsuura, M.; Yamamoto, A.; Kishikawa, Y. Photoredox-Catalyzed Hydrodifluoroalkylation of Alkenes Using Difluorohaloalkyl Compounds and a Hantzsch Ester. *J. Org. Chem.* **2017**, *82*, 5469. (d) Zhou, Q.; Ruffoni, A.;

Gianatassio, R.; Fujiwara, Y.; Sella, E.; Shabat, D.; Baran, P. S. Direct Synthesis of Fluorinated Heteroarylether Bioisosteres. *Angew. Chem., Int. Ed.* **2013**, *52*, 3949. (e) Jung, J.; Kim, E.; You, Y.; Cho, E. J. Visible Light-Induced Aromatic Difluoroalkylation. *Adv. Synth. Catal.* **2014**, *356*, 2741. (f) Lemos, A.; Lemaire, C.; Luxen, A. Progress in Difluoroalkylation of Organic Substrates by Visible Light Photoredox Catalysis. *Adv. Synth. Catal.* **2019**, *361*, 1500. (g) Geri, J. B.; Wade Wolfe, M. M.; Szymczak, N. K. The Difluoromethyl Group as a Masked Nucleophile: A Lewis Acid/Base Approach. *J. Am. Chem. Soc.* **2018**, *140*, 9404. (h) Luo, C.; Bandar, J. S. Selective Defluoroallylation of Trifluoromethylarenes. *J. Am. Chem. Soc.* **2019**, *141*, 14120.

[6] (a) Heck, R. F.; Nolley, J. P. Palladium-catalyzed vinylic hydrogen substitution reactions with aryl, benzyl, and styryl halides. *J. Org. Chem.* **1972**, *37*, 2320. (b) Link, J. T. The Intramolecular Heck Reaction. In *Organic Reactions*, Overman, L. E. Ed.; Wiley, New Jersey, 2002, Vol. 60, pp 157-561.

[7] (a) Sonogashira, K.; Tohda, Y.; Hagihara, N. A convenient synthesis of acetylenes: catalytic substitutions of acetylenic hydrogen with bromoalkenes, iodoarenes and bromopyridines. *Tetrahedron Lett.* **1975**, *16*, 4467. (b) Chinchilla, R.; Nájera, C. The Sonogashira Reaction: A Booming Methodology in Synthetic Organic Chemistry. *Chem. Rev.* **2007**, *107*, 874.

[8] Prier, C. K.; Rankic, D. A.; MacMillan, D. W. C. Visible Light Photoredox Catalysis with Transition Metal Complexes: Applications in Organic Synthesis. *Chem. Rev.* **2013**, *113*, 5322.

[9] (a) Miyaura, N.; Suzuki, A. Palladium-Catalyzed Cross-Coupling Reactions of Organoboron Compounds. *Chem. Rev.* **1995**, *95*, 2457.

[10] (a) Baggett, N. In *Comprehensive Organic Chemistry*; Stoddart, J. F., Ed.; Pergamon Press: New York, 1979; Vol. 1, pp 799-850. (b) Freedman, H. H.; Dubois, R. A. An Improved Williamson Ether Synthesis Using Phase Transfer Catalysis. *Tetrahedron Lett.* **1975**, *16*, 3251.

[11] The synthesis of alkene **9** is shown in Scheme 7 and described in detail in reference 2. Alkyne **10** was prepared by the analogous route starting with propargyl alcohol instead of allyl alcohol. Standard conditions were employed to couple amine **11** with the acids **9** and **10**, producing **5** and **6**. The alkyne **6** was converted to boronic acid **7** and under standard hydroboration/oxidation conditions, and the boronate ester **8** by hydroborylation.

[12] (a) Milne, J. A.; Buchwald, S. L. An Extremely Active Catalyst for the Negishi Cross-Coupling Reaction. *J. Am. Chem. Soc.* **2004**, *126*, 13028. (b) Martin, R.; Buchwald, S. L. Palladium-Catalyzed Suzuki-Miyaura Cross-Coupling Reactions Employing Dialkylbiaryl Phosphine Ligands. *Acc. Chem Res.* **2008**, *41*, 4161.

[13] Model boronate ester **26** was prepared by hydrogenation of **36** followed by ether formation with propargyl bromide and then hydroborylation. The quinoxaline **27** is an intermediate in the synthesis of **11**.

[14] (a) Zhou, J.; Fu, G. C. Suzuki Cross-Couplings of Unactivated Secondary Alkyl Bromides and Iodides. *J. Am. Chem. Soc.* **2004**, *126*, 1340. (b) Rosen, B. M.; Quasdorf, K. W.; Wilson, D. A.; Zhang, Na.; Resmerita, A.-M.; Garg, N. K.; Percec, V. Nickel-Catalyzed Cross-Couplings Involving Carbon-Oxygen Bonds. *Chem. Rev.* **2011**, *111*, 1346.

[15] Intermediate **12** was prepared by the coupling of carbamate **13** (Scheme 7) with amine **6** from reference 2, followed by cross metathesis with 1,4-dibromobut-2-ene.

[16] The NMR data for impurity **29** was consistent with the structure drawn but was not unambiguously determined. Cyclization could also occur at the carbamate oxygen.

[17] Shi, G.; Cai, W. δ,ε-Unsaturated β,β-Difluoro-α-keto Esters: Novel Synthesis and Utility as Precursors of β,β-Difluoro-α-amino Acids. *J. Org. Chem.* **1995**, *60*, 6289.

[18] Chen, M. S.; White, M. C. A Sulfoxide-Promoted, Catalytic Method for the Regioselective Synthesis of Allylic Acetates from Monosubstituted Olefins via C−H Oxidation. *J. Am. Chem. Soc.* **2004**, *126*, 1346.

[19] McCabe Dunn, J. M; Duran-Capece, A.; Meehan, B.; Ulis, J.; Iwama, T.; Gloor, G.; Wong, G.; Bekos, E. The Safe Use of Sodium Hydride on Scale: The Process Development of a Chloropyrimidine Displacement. *Org. Process Res. Dev.* **2011**, *15*, 1442.

[20] Yang. D; Wong, M.-K; Yip, Y.-C. Epoxidation of Olefins Using Methyl(trifluoromethyl)dioxirane Generated in Situ. *J. Org. Chem.* **1995**, *60*, 3887.

[21] VanRheenen, V.; Kelly, R. C.; Cha, D. Y. An improved catalytic OsO_4 oxidation of olefins to *cis*-1,2-glycols using tertiary amine oxides as the oxidant. *Tetrahedron Lett.* **1976**, *17*, 1973.

[22] Another pathway through dimerization of **51** prior to S_NAr is possible, but the dimer of **51** is not observed.

[23] The estimated error range tor the DFT calculations is 1 kcal/mol. See Supporting Information for further details.

[24] Castro, B. R. Replacement of alcoholic hydroxyl groups by halogens and other nucleophiles via oxyphosphonium intermediates. In *Organic Reactions*, Dauben, W. G. Ed.; Wiley, New York, 1983, Vol. 29, pp 1–162.

[25] A computational study was initiated in an effort to understand the basis for the observed differences in the rate of cyclization versus the rate of hydrolysis for the allylic bromide stereoisomers. Due to the structural complexity and conformational flexibility of allylic bromide stereoisomers, it was not possible through the computational analysis to determine the basis for the observed selectivity with a high degree of confidence.

[26] International Conference on Harmonisation of Technical Requirements for Registration of Pharmaceuticals for Human Use; ICH QM7 *Assessment and control of DNA reactive (mutagenic) Impurities in Pharmaceuticals*, Geneva, Switzerland, 2015.

[27] Popkin, M. E.; Borman, P. J.; Omer, B. A.; Curran, T.; Kallemeyn, J. M. Enhanced Approaches to the Identification, Evaluation, and Control of Impurities. *J. Pharm. Innov.* **2019**, *14*, 176.

[28] Charges for this three-step sequence (g/g, or kg/kg or equiv.) are relative to **31** as the basis.